Influence of the Polyakov loop on the chiral phase transition in the two flavor chiral quark model

G. Markó*

Department of Atomic Physics, Eötvös University, H-1117 Budapest, Hungary

Zs. Szép†

Statistical and Biological Physics Research Group of the Hungarian Academy of Sciences, H-1117 Budapest, Hungary

(Received 1 June 2010; revised manuscript received 9 August 2010; published 24 September 2010)

The $SU(2)_L \times SU(2)_R$ chiral quark model consisting of the $(\sigma, \vec{\pi})$ meson multiplet and the constituent quarks propagating on the homogeneous background of a temporal gauge field is solved at finite temperature and quark baryon chemical potential μ_q using an expansion in the number of flavors N_f, both in the chiral limit and for the physical value of the pion mass. Keeping the fermion propagator at its tree level, several approximations to the pion propagator are investigated. These approximations correspond to different partial resummations of the perturbative series. Comparing their solution with a diagrammatically formulated resummation relying on a strict large-N_f expansion of the perturbative series, one concludes that only when the local part of the approximated pion propagator resums infinitely many orders in $1/N_f$ of fermionic contributions a sufficiently rapid crossover transition at $\mu_q = 0$ is achieved allowing for the existence of a tricritical point or a critical end point in the $\mu_q - T$ phase diagram. The renormalization and the possibility of determining the counterterms in the resummation provided by a strict large-N_f expansion are investigated.

DOI: 10.1103/PhysRevD.82.065021 PACS numbers: 11.10.Wx, 11.30.Rd, 12.38.Cy

I. INTRODUCTION

The low-energy effective models of the QCD, such as the Nambu–Jona-Lasinio (NJL) model [1] and the linear sigma model [also called chiral quark or quark-meson (QM) model] [2] are based on the global chiral symmetry of the QCD. They proved to be very useful in qualitative understanding of many aspects related to the spontaneous breaking of the chiral symmetry and its restoration at finite temperature and density, but share as a major drawback the lack of the confinement property. As a consequence of the absence of gluonic effective degrees of freedom and due to the lack of color clustering [3] there are unsuppressed contributions of constituent quarks in the low-temperature phase. Both features, which are in fact related, alter the reliability of the quantitative thermodynamic predictions of these models, such as the equation of state or the location of the critical end point (CEP) in the $\mu_q - T$ phase diagram.

Since the QCD phase transition involves both the restoration of chiral symmetry measured by the evaporation of the chiral condensate $\langle \bar{\psi}\psi \rangle$ and the liberation of quarks and gluons encoded in the change of the Polyakov loop Φ, much effort was devoted to understand the relation between the chiral and deconfinement phase transitions. An argument by Casher [4] states that in the vacuum, that is at $\mu_q = T = 0$, confinement implies the breaking of the chiral symmetry. The connection between $\langle \bar{\psi}\psi \rangle$ and Φ is revealed by the spectral density of the Dirac operator $\rho(\lambda)$. In the vacuum the Banks-Casher relation $\rho(0) = \langle \bar{\psi}\psi \rangle / \pi$ [5] states that the spectral density of the Dirac operator in the deep infrared is proportional to the quark condensate. Finite temperature lattice studies at $\mu_q = 0$ show that the connection between chiral symmetry and confinement suggested by Casher's argument holds. The infrared part of $\rho(\lambda)$ undergoes a pronounced change as one crosses from the confined to the deconfined phase [6,7]. As shown recently in [8], the phase of the Polyakov loop Φ, which can be expressed as a spectral sum of eigenvalues and eigenvectors of the Dirac operator with different boundary conditions, receives its main contribution from the infrared end of $\rho(\lambda)$. It is generally true for both $N_c = 2$ and $N_c = 3$ that at high temperature the fermion determinant favors the sector where the Polyakov loop lies along the positive real axis [6,7]. For this type of configuration in which the phase of Φ vanishes the chiral symmetry is restored, because a sizable gap develops in the spectral density of the Dirac operator which implies in view of the Banks-Casher relation $\langle \bar{\psi}\psi \rangle = 0$. For configurations in which the phase of the Polyakov loop is not vanishing, the chiral symmetry is not restored, as observed in the lattice study of the quenched QCD [9] and also by using a random matrix model calculation [10].

Casher's argument suggests that the temperature T_d for the deconfinement phase transition is somewhat lower than the restoration temperature T_χ of the chiral symmetry. As explained in [11] at finite density Casher's argument could fail, so that it does not contradict the existence of a dense phase in which at a given temperature chiral symmetry is restored while quarks remain confined. Such a phase can exist inside the so-called quarkyonic phase, which was

*smarkovics@hotmail.com
†szepzs@achilles.elte.hu

suggested as a new phase of the QCD at finite temperature and density, based on its existence within a large-N_c analysis [12].

In the Polyakov-loop extended NJL model (PNJL) where the coupling of the Polyakov loop to the quark sector is achieved by the propagation of the quarks on a constant temporal gauge field background, the simultaneous crossover-type transition of deconfinement and chiral restoration was obtained [13]. As shown in [14,15] this model is able to reproduce the main features of the quenched lattice result of [9]. The phase transition was recently intensively investigated in the PNJL model with two [16–20] and three flavors [21–23], also in the nonlocal formulation of the model [24,25]. The interplay between chiral and deconfinement transitions was investigated in the PNJL model using large-N_c expansion in [26].

By coupling the Polyakov loop to the quark degrees of freedom of the QM model the thermodynamics of the resulting Polyakov quark-meson model (PQM) was studied for two [27–32] and three quark flavors [33–35]. The effect of a strong magnetic field expected to be generated in the LHC in noncentral high-energy heavy ion collisions on the chiral and deconfining phase transitions was studied recently in [36] within the PQM model with two flavors. The possibility of coupling the Polyakov loop to meson models without quarks was considered in [37,38].

The coupling of the Polyakov loop to the chiral effective models mimics the effect of confinement by statistically suppressing at low temperature the contribution of one- and two-quark states relative to the three-quark states. This feature makes the Polyakov-loop extended effective models more appropriate for the description of the low-temperature phase and for quantitative comparison with the thermodynamic observables on the lattice [27,33,39]. Better agreement is expected up to $T \simeq (1.5 - 2)T_c$ above which the transverse gluonic degrees of freedom dominate in thermodynamic quantities, such as the pressure, over the longitudinal ones represented by the Polyakov loop.

Despite this success, one should keep in mind that the solution of the Polyakov-loop extended effective models is mainly obtained in the lowest one-loop (trace-log) order of the fermionic sector, hence studying their stability against inclusion of higher loops would be certainly of interest. Some approximations to the PQM model [27,28,33–35] neglect the fermionic vacuum fluctuations and by treating the mesonic potential at tree level, completely disregard quantum effects in the mesonic sector. The effect of including the quantum fluctuation in the PQM model was recently studied in [29,30,32] using functional renormalization group methods.

In this work we would like to address two questions using large-N_f approximation to the $SU(2)_L \times SU(2)_R \simeq O(4)$ model. The first one is to what extent the inclusion of the Polyakov loop modifies the $\mu_q - T$ phase diagram obtained previously in [40] in the chiral limit of the two flavor QM using the large-N_f approximation. The second one concerns the effect of different partial resummations on the quantitative results. To this end several approximate resummations of the perturbative series will be investigated and the obtained results compared.

The paper is organized as follows. In Sec. II we overview some basic facts about the Polyakov loop, including different forms of the effective potential and we introduce and parametrize the PQM model, presenting also the approximations exploited for its solution. The renormalization of the model and the determination of the counterterms is discussed in Sec. III. In Sec. IV we present the numerical results on the $\mu_q - T$ phase diagram obtained in the chiral limit and for the physical value of the pion mass by using different forms of the Polyakov-loop effective potential and various approximations to the resummed pion propagator. Section V is devoted to discussion and summary.

II. THE PQM MODEL WITHIN A LARGE-N_f APPROXIMATION

A. The Polyakov loop as an order parameter

We shortly review a few well-known facts about the Polyakov loop incorporated as a new effective degree of freedom in the chiral quark model. This is usually done by considering the propagation of quarks on the homogeneous background of a temporal gauge field $A_0(x)$. At finite temperature $T = 1/\beta$, after analytical continuation to imaginary time $t \to i\tau$, $A_0 \to iA_4$, the temporal component of the Euclidean gauge field A_4 enters in the definition of the Polyakov-loop operator (path ordered Wilson line in temporal direction) $L(\vec{x})$ and its Hermitian (charge) conjugate $L^\dagger(\vec{x})$

$$\begin{aligned} L(\vec{x}) &= \mathcal{P}\exp\left[i\int_0^\beta d\tau A_4(\tau,\vec{x}) \right], \\ L^\dagger(\vec{x}) &= \mathcal{P}\exp\left[-i\int_0^\beta d\tau A_4^*(\tau,\vec{x}) \right], \end{aligned} \tag{1}$$

which are matrices in the fundamental representation of the $SU(N_c)$ color gauge group ($N_c = 3$). In the so-called Polyakov gauge, the temporal component of the gauge field is time independent and can be gauge rotated to a diagonal form in the color space $A_{4,d}(\vec{x}) = \phi_3(\vec{x})\lambda_3 + \phi_8(\vec{x})\lambda_8$ [41–43], where λ_3, λ_8 are the two diagonal Gell-Mann matrices. Then the Polyakov-loop operator simplifies

$$L(\vec{x}) = \mathrm{diag}(e^{i\beta\phi_+(\vec{x})}, e^{i\beta\phi_-(\vec{x})}, e^{-i\beta(\phi_+(\vec{x})+\phi_-(\vec{x}))}), \tag{2}$$

where $\phi_\pm(\vec{x}) = \pm\phi_3(\vec{x}) + \phi_8(\vec{x})/\sqrt{3}$, with a similar form for the conjugate $L^\dagger(\vec{x})$.

Topologically nontrivial gauge transformations $U(\tau,\vec{x}) \in SU(N_c)$ that are periodic up to a twist, that is $U(\tau+\beta,\vec{x}) = zU(\tau,\vec{x})$ were introduced in [44], where z is an element of the center of the $SU(N_c)$ group

which is isomorphic with $\mathbb{Z}_{N_c} = \{z | z = \exp(2\pi n i/N_c), n = 0, 1, \ldots, N_c - 1\}$, the cyclic group of order N_c. Under such transformations the color trace of the Polyakov-loop operator and its conjugate, that is $l(x) = \mathrm{tr}_c L(\vec{x})/N_c$ and $l^\dagger(x) = \mathrm{tr}_c L^\dagger(\vec{x})/N_c$, are transformed by an element of the center $l(x) \to z l(x)$, $l^\dagger(x) \to z^* l^\dagger(x)$. Consequently, in the pure gauge theory, which has an exact $\mathbb{Z}_{N_c}$ global symmetry, the thermal expectation value of the traced Polyakov-loop operator and its conjugate,

$$\Phi(\vec{x}) = \frac{1}{N_c}\langle \mathrm{tr}_c L(\vec{x})\rangle, \qquad \bar{\Phi}(\vec{x}) = \frac{1}{N_c}\langle \mathrm{tr}_c L^\dagger(\vec{x})\rangle, \tag{3}$$

are order parameters for the center symmetry and must vanish if the symmetry is unbroken. However, the Polyakov loop $\Phi(\vec{x})$ and its conjugate $\bar{\Phi}(\vec{x})$ can acquire a nonvanishing value, signaling the spontaneous breaking of the $\mathbb{Z}_{N_c}$ symmetry. These complex quantities can be regarded as order parameters of the deconfinement phase transition, because the free energy of a heavy (static) quark-antiquark pair with spatial separation $\vec{r} = \vec{x} - \vec{y}$ is related to the expectation value of the correlator of the traced Polyakov-loop operator for which cluster decomposition is expected to hold at infinite separation

$$\exp[-\beta F_{q\bar{q}}(\vec{r})] = \frac{1}{N_c^2}\langle L(\vec{x}) L^\dagger(\vec{x})\rangle \to \Phi(\vec{x})\bar{\Phi}(\vec{y}). \tag{4}$$

When $\Phi(\vec{x})$, $\bar{\Phi}(\vec{y}) = 0$ then $F_{q\bar{q}}(\vec{r}) \to \infty$, and when $\Phi(\vec{x})$, $\bar{\Phi}(\vec{y}) \neq 0$ then $F_{q\bar{q}}(\vec{r})$ is finite, which means confinement and deconfinement, respectively [45,46].

In the presence of dynamical fermions the $\mathbb{Z}_{N_c}$ symmetry is not exact anymore. Nevertheless, the Polyakov loop gives through its distribution information about the confinement (low T) or deconfinement phase (high T) of the system both in a canonical or grand-canonical formulation of the QCD [47,48]. Since its absolute value can be related to the free energy difference between two systems, one containing the quark-antiquark source pair and the other not containing it, by renormalizing the free energy a renormalized Polyakov loop can be defined [49], which provides information on the temperature of the deconfinement phase transition.

B. The mean-field Polyakov-loop potentials

In the mean-field approximation $\Phi(x)$ and $\bar{\Phi}(x)$ are replaced by x-independent constant fields which satisfy $|\Phi| = |\bar{\Phi}|$ at vanishing chemical potential. We review here several forms and some basic features of the mean-field effective potential for the Polyakov loop frequently used in the literature. This effective potential will be incorporated in the thermodynamic potential of the PQM model. The simplest effective potential is of a Landau type, constructed with terms consistent with the $\mathbb{Z}_3$ symmetry [50]:

$$\beta^4 \mathcal{U}_{\mathrm{poly}}(\Phi, \bar{\Phi}) = -\frac{b_2(T)}{2}\Phi\bar{\Phi} - \frac{b_3}{6}(\Phi^3 + \bar{\Phi}^3) + \frac{b_4}{4}(\Phi\bar{\Phi})^2, \tag{5}$$

where the temperature-dependent coefficient which makes spontaneous symmetry breaking possible is

$$b_2(T) = a_0 + a_1\left(\frac{T_0}{T}\right) + a_2\left(\frac{T_0}{T}\right)^2 + a_3\left(\frac{T_0}{T}\right)^3. \tag{6}$$

T_0 is the transition temperature of the confinement/deconfinement phase transition, in the pure gauge theory $T_0 = 270$ MeV. The parameters a_i, $i = 0, \ldots, 3$ and b_3, b_4 determined in [51] reproduce the data measured in pure $SU(3)$ lattice gauge theory [52] for pressure, and entropy and energy densities. The minimum of this potential is at $\Phi = 0$ for low temperature and $\Phi \to 1$ for $T \to \infty$ in accordance with the definitions (1) and (3). However, when using this potential in either the PNJL or the PQM models the minimum of the resulting thermodynamic potential is at $\Phi > 1$ for $T \to \infty$ and also leads to negative susceptibilities [24].

An effective potential for the Polyakov loop inspired by a strong-coupling expansion of the lattice QCD action was derived in [13,53]. Using the part coming from the $SU(3)$ Haar measure of group integration an effective potential was constructed in [54,55]

$$\beta^4 \mathcal{U}_{\log}(\Phi, \bar{\Phi}) = -\tfrac{1}{2}a(T)\Phi\bar{\Phi} + b(T)\ln[1 - 6\Phi\bar{\Phi} + 4(\Phi^3 + \bar{\Phi}^3) - 3(\Phi\bar{\Phi})^2], \tag{7}$$

with the temperature-dependent coefficients

$$a(T) = a_0 + a_1\left(\frac{T_0}{T}\right) + a_2\left(\frac{T_0}{T}\right)^2, \qquad b(T) = b_3\left(\frac{T_0}{T}\right)^3. \tag{8}$$

The parameters a_i, $i = 0, 1, 2$ and b_3 determined in [54] reproduce the thermodynamic quantities in the pure $SU(3)$ gauge theory measured on the lattice. The use of this effective potential cures the problem with negative susceptibilities [24] and since the logarithm in $\mathcal{U}_{\log}(\Phi, \bar{\Phi})$ diverges as $\Phi, \bar{\Phi} \to 1$ it will also guarantee that $\Phi, \bar{\Phi} \to 1$ for $T \to \infty$.

A third effective potential is the one determined in Refs. [13,53]:

$$\beta \mathcal{U}_{\mathrm{Fuku}}(\Phi, \bar{\Phi}) = -b[54 e^{-a/T}\Phi\bar{\Phi} + \ln[1 - 6\Phi\bar{\Phi} + 4(\Phi^3 + \bar{\Phi}^3) - 3(\Phi\bar{\Phi})^2]], \tag{9}$$

where a controls the temperature of the deconfinement phase transition in pure gauge theory, while b controls the weight of gluonic effects in the transition. In this case, the parameters $a = 664$ MeV and $b = (196.2\ \mathrm{MeV})^3$ are obtained from the requirement of having a first order transition at about $T = 270$ MeV [27,56].

It was shown in [56] that there is little difference in the pressure calculated from the three effective potentials

for the Polyakov loop in their validity region up to $T \simeq (1.5-2)T_c$. The presence of dynamical quarks influences an effective treatment based on the Polyakov loop which in this case is not an exact order parameter. Defining effective Polyakov-loop potentials for nonvanishing chemical potential when $|\Phi| \neq |\bar{\Phi}|$ is somewhat ambiguous [27]. In the present analysis we will use at $\mu_q \neq 0$ the $\mathbb{Z}_3$ symmetric Polyakov-loop potentials given above. The effect of the dynamical quarks was modeled by considering the N_f and μ_q dependence of the T_0 parameter of the Polyakov-loop effective potential. Using renormalization group arguments this dependence was parametrized in [27] to be of the form $T_0(\mu_q, N_f) = T_\tau \exp(-1/(\alpha_0 b(\mu_q)))$. The parameters were chosen to have $T_0(\mu_q = 0, N_f = 2) = 208.64$ MeV. When using the polynomial and logarithmic effective potential for the Polyakov loop given in (5) and (7) we will consider in addition to $T_0 = 270$ MeV two more cases, one with a constant value $T_0 = 208$ MeV and the other with the above-mentioned μ_q-dependent T_0 taken at $N_f = 2$.

C. Constructing the grand potential of the PQM in a "Φ-derivable" approximation

The Lagrangian of the $SU(2)_L \times SU(2)_R$ chiral quark model [2] is written in the usual matrix form [57,58] by introducing two $N_f \times N_f$ matrices

$$M(x) = \frac{\sigma(x)}{\sqrt{2N_f}}\mathbb{1} + iT^a\pi^a(x),$$
$$M_5(x) = \frac{\sigma(x)}{\sqrt{2N_f}}\mathbb{1} + i\gamma_5 T^a\pi^a(x), \tag{10}$$

in terms of which one has

$$\mathcal{L} = \mathrm{tr}_f[\partial_\mu M^\dagger \partial^\mu M - m^2 M^\dagger M] - \frac{\lambda}{6N}[\mathrm{tr}_f(M^\dagger M)]^2 + N_f h\sigma + \bar{\psi}(i\gamma^\mu D_\mu - \tilde{g}M_5)\psi + \text{c.t.}, \tag{11}$$

where in the mesonic part we have introduced an explicit symmetry breaking term and "c.t." stands for counterterms. After performing the trace, one can see that without the fermionic term the Lagrangian (11) is that of the $O(N)$ model, which describes the system of sigma and $N-1$ pion fields and is appropriately parametrized for a large-N treatment [59]. Vanishing background is considered for the spatial components of the gauge field and a constant mean-field A_0 for the temporal component, so that the covariant derivative is $D_\mu = \partial_\mu - i\delta_{\mu 0}A_0$. The trace in (11) is to be taken in the flavor space and to simplify notations the flavor, color, and Dirac indices of the fermionic fields ψ, $\bar{\psi}$ are not indicated. The $SU(N_f)$ generators in the fundamental representation T^a $(a = 1, \ldots, N_f^2 - 1)$ satisfy the normalization condition $\mathrm{tr}_f(T^a T^b) = \delta^{ab}/2$. Some rescaling with $N_f = \sqrt{N}$ was done and since in the mesonic sector we only want to increase the number of pions we do not introduce another invariant, $\mathrm{tr}_f[(M^\dagger M)^2]$, which for $N_f > 2$ is independent of $[\mathrm{tr}_f(M^\dagger M)]^2$. For a recent treatment of the $U(N_f)_L \times U(N_f)_R$ meson model having both invariants see [60].

The constituent quarks become massive only after spontaneous/explicit symmetry breaking. In (11) the sigma field is shifted by the vacuum expectation value v as $\sigma \to v\sqrt{N} + \sigma$, where on the right-hand side of the arrow σ denotes the fluctuating part of the original field. Then evaluating the trace, one obtains

$$\begin{aligned}\mathcal{L} = &-N\left[\frac{\lambda}{24}v^4 + \frac{1}{2}m^2v^2 - hv\right] - \sqrt{N}\left[\frac{\lambda}{6}v^3 + m^2v - h\right]\sigma \\ &+ \frac{1}{2}[(\partial\sigma)^2 + (\partial\vec{\pi})^2] - \frac{1}{2}m_{\sigma 0}^2\sigma^2 - \frac{1}{2}m_{\pi 0}^2\vec{\pi}^2 - \frac{\lambda v}{6\sqrt{N}}\sigma\rho^2 \\ &- \frac{\lambda}{24N}\rho^4 + \bar{\psi}[(i\partial^\mu + \delta^{\mu 0}A_0)\gamma_\mu - m_q]\psi \\ &- \frac{g}{\sqrt{N}}[\bar{\psi}(\sigma + i\sqrt{2N_f}\gamma_5 T^a\pi^a)]\psi + \text{c.t.},\end{aligned} \tag{12}$$

where $\rho^2 = \sigma^2 + \vec{\pi}^2$. Here a rescaled Yukawa coupling $g = \tilde{g}\sqrt{N/(2N_f)}$ was introduced in order to assure the finiteness of the tree-level quark mass $m_q = gv$ in the $N \to \infty$ limit. In this limit, due to the N_f scaling of the vacuum expectation value of the sigma field in (10) and of the coupling λ in (11) the tree-level sigma and pion masses $m_{\sigma 0}^2 = m^2 + \lambda v^2/2$ and $m_{\pi 0}^2 = m^2 + \lambda v^2/6$ are also finite.

After continuation to imaginary time, the grand partition function Z and the grand potential $\Omega(T, \mu_B)$ of the spatially uniform system defined by (12) are introduced as follows:

$$Z = \mathrm{tr}\{\exp[-\beta(H_0(A_4) + H_{\text{int}} - \mu_B Q_B)]\} = e^{-\beta\Omega}, \tag{13}$$

where μ_B is the baryon chemical potential. H_{int} is the interacting part of the Hamiltonian constructed from (12). With the help of H_0, the quadratic part of the Hamiltonian at vanishing A_4, one can define the A_4-dependent free Hamiltonian $H_0(A_4)$, which for two quark flavors u and d reads as

$$H_0(A_4) = H_0 + \int d^3x[iu_i^\dagger(x)A_{4,ij}u_j(x) + id_i^\dagger(x)A_{4,ij}d_j(x)], \tag{14}$$

where $A_4 = \mathrm{diag}(\phi_+, \phi_-, -(\phi_+ + \phi_-))$ is diagonal in color space and i, j denotes color indices. In (13) Q_B is the conserved baryon charge which can be written in terms of the particle number operators as $Q_B = \frac{1}{3}\times \sum_{i=1}^3 N_{q,i}$, with $N_{q,i} = N_{u,i} + N_{d,i} - N_{\bar{u},i} - N_{\bar{d},i}$ and e.g. $N_{u,i} = \int d^3x(u_i^\dagger u_i + d_i^\dagger d_i)$. Then combining $H_0(A_4)$ and $\mu_B Q_B$ one can see that the effect of fermions propagating on the constant background A_4, diagonal in the color space, is like having imaginary chemical potential for color.

Following Ref. [61] one introduces color-dependent chemical potential for fermions

$$\mu_{1,2} = \mu_q - i\phi_-, \qquad \mu_3 = \mu_q + i(\phi_+ + \phi_-), \quad (15)$$

where $\mu_q = \mu_B/3$ is the quark baryon chemical potential. Then, introducing the notation $\mathcal{H} = H_0 - \sum_{i=1}^{3} \mu_i N_{q,i}$, one can write Z as a path integral over the fields, generically denoted by Ψ

$$Z = e^{-\beta\Omega_0} \frac{\int[\mathcal{D}\Psi]\{e^{-\beta\mathcal{H}}\mathcal{P}\exp[-\int_0^\beta d\tau H_{\rm int}(\tau)]\}}{\int[\mathcal{D}\Psi]e^{-\beta\mathcal{H}}}, \quad (16)$$

where Ω_0 is the grand potential of the unperturbed system with fermions having color-dependent chemical potential

$$e^{-\beta\Omega_0} = \int[\mathcal{D}\Psi]e^{-\beta\mathcal{H}}. \quad (17)$$

In the one-particle irreducible (1PI) formalism the grand potential is given by the sum of the grand potential of the unperturbed system and of perturbative quantum corrections represented by closed loops constructed with the tree-level (free) propagators. In the Φ-derivable approximation of Ref. [62], also called two-particle irreducible (2PI) approximation, the grand potential is a functional of the full propagators and field expectation values, and is of the following form:

$$\begin{aligned}\beta\Omega[G_\pi, G_\sigma, G, v, \Phi, \bar\Phi] &= U(\Phi,\bar\Phi) + \frac{N}{2}m^2v^2 + N\frac{\lambda}{24}v^4 - Nhv - (N-1)\\ &\times\frac{i}{2}\int_k[\ln G_\pi^{-1}(k) + D_\pi^{-1}(k)G_\pi(k)] - \frac{i}{2}\int_k[\ln G_\sigma^{-1}(k)\\ &+ D_\sigma^{-1}(k)G_\sigma(k)] + \sqrt{N}i\,\mathrm{tr}_{D,c}\int_k[\ln G^{-1}(k)\\ &+ D^{-1}(k)G(k)] + \Gamma_{\rm 2PI}[G_\pi, G_\sigma, G, v, \Phi, \bar\Phi] + \text{c.t.}, \quad (18)\end{aligned}$$

where the trace is taken in Dirac and color space. $U(\Phi, \bar\Phi)$ is a particular version of the effective Polyakov-loop potential reviewed in Sec. II B; the tree-level propagators of the pion, sigma, and constituent quark fields are

$$\begin{aligned} iD_\pi^{-1}(k) &= k^2 - m_{\pi 0}^2, \qquad iD_\sigma^{-1}(k) = k^2 - m_{\sigma 0}^2,\\ iD^{-1}(k) &= \not{k} - m_q, \end{aligned} \quad (19)$$

while G_π, G_σ, and G are the respective full propagators. $\Gamma_{\rm 2PI}[G_\pi, G_\sigma, G, v, \Phi, \bar\Phi]$ denotes the set of 2PI skeleton diagrams constructed with full propagators, which to $\mathcal{O}(1/\sqrt{N})$ accuracy is given by

$$\begin{aligned}\Gamma_{\rm 2PI}[G_\pi, G_\sigma, G, v, \Phi, \bar\Phi] &= N\frac{\lambda}{24}\left(\int_k G_\pi(k)\right)^2 + \frac{\lambda}{12}\int_k G_\pi(k)\int_p G_\sigma(p) - \frac{\lambda}{12}i\int_k \Pi(k) - \frac{i}{2}\int_k \ln\left(1 - \frac{\lambda}{6}\Pi(k)\right)\\ &- \frac{\lambda}{6}v^2\int_k G_\sigma(k) + \frac{\lambda}{6}v^2\int_k \frac{G_\sigma(k)}{1 - \lambda\Pi(k)/6} - \sqrt{N}\frac{g^2}{2}i\,\mathrm{tr}_{D,c}\int_k\int_p \gamma_5 G(k)\gamma_5 G(k+p)G_\pi(p)\\ &+ \frac{g^2}{2\sqrt{N}}i\,\mathrm{tr}_{D,c}\int_k\int_p G(k)G(k+p)G_\sigma(p), \end{aligned} \quad (20)$$

where the notation $\Pi(k) = -i\int_p G_\pi(p)G_\pi(k+p)$ was introduced. The mesonic part of $\Gamma_{\rm 2PI}$ contains the 2PI diagrams of the $O(N)$ model as given in Eq. (2.13) and Figs. 2 and 4 of [63] and also in Eq. (48) and Fig. 2 of [64]. We see that the contribution of the fermions which goes with fractional powers of N intercalates between the leading order (LO) and next-to-leading order (NLO) contributions of the pions, which go with integer powers of N. This can be also seen by comparing the expression of the pion propagator derived in (29) with Eqs. (53) and (54) of [64].

We use the imaginary time formalism of the finite temperature field theory in which the four-momentum is $k = (i\omega_n, \mathbf{k})$. The Matsubara frequencies are $\omega_n = 2\pi nT$ for bosons while for fermions they depend also on the color due to the color-dependent chemical potential μ_i introduced in (15) and are given by $\omega_n = (2n+1)\pi T - i\mu_i$. The meaning of the integration symbol in (20) is

$$\int_k = iT\sum_n\int_{\mathbf{k}} \equiv iT\sum_n\int\frac{d^3\mathbf{k}}{(2\pi)^3}. \quad (21)$$

The dependence on Φ and $\bar\Phi$ of the fermionic trace-log term in the grand potential Ω and of the quark-pion setting sun in $\Gamma_{\rm 2PI}$ results from the fact that, as shown in the Appendix between Eqs. (A1) and (A5), as well as between Eqs. (A35) and (A37), respectively, after performing the Matsubara sum the color trace can be expressed in closed form in terms of the mean-field ($\vec{x}$-independent) Polyakov loop Φ and its conjugate $\bar\Phi$.

What we evaluate in this work is not the grand potential (20), but rather its derivatives, that is the equations for the two-point functions and the field equations, which are given by the stationary conditions

$$\frac{\delta\Omega}{\delta G} = \frac{\delta\Omega}{\delta G_\pi} = \frac{\delta\Omega}{\delta G_\sigma} = \frac{\delta\Omega}{\delta v} = \frac{\delta\Omega}{\delta\Phi} = \frac{\delta\Omega}{\delta\bar\Phi} = 0. \quad (22)$$

In each of these equations we will keep the contribution of the fermions only at the leading order in the large-N_f expansion. The LO contribution of the fermions is $\mathcal{O}(\sqrt{N})$ in the field equations of Φ and $\bar{\Phi}$, $\mathcal{O}(1)$ in the equation for the fermion propagator G, and $\mathcal{O}(1/\sqrt{N})$ in the remaining equations, that is the field equation of v, and the equations of G_π and G_σ.

It is easy to see that the third and fourth terms on the right-hand side of (20) do not contribute to any of the equations at the order of interest, and that the second term contributes only in the equation for the sigma propagator

$$iG_\sigma^{-1}(p) = iD_\sigma^{-1}(p) + \frac{\lambda v^2}{3} - \frac{\lambda}{6}\int_k G_\pi(k) - \frac{\lambda v^2}{3}\frac{1}{1-\lambda\Pi(p)/6} - \frac{ig^2}{\sqrt{N}}\,\mathrm{tr}_{D,c}\int_k G(k)G(k+p) + \text{c.t.} \quad (23)$$

In fact, the equation for G_σ decouples, in the sense that G_σ will not appear in any of the remaining five equations. Nevertheless, it plays an important role in the parametrization of the model, as will be shown in Sec. II E.

D. Approximations made to solve the model

In this work we use some approximations to solve the set of coupled equations coming from (22).

(1) As a first approximation we disregard the self-consistent equation for the fermions arising from $\delta\Omega/\delta G = 0$, that is

$$iG^{-1}(k) = iD^{-1}(k) - ig^2\int_p \gamma_5 G(p)\gamma_5 G_\pi(p-k) + \text{c.t.}, \quad (24)$$

and simply use in the remaining five equations the tree-level fermion propagator $D(k)$. A study based on the solution of the self-consistent equation for the fermion propagator is left for a forthcoming publication.

Within this approximation the field equation for v, hereinafter called equation of state (EoS), and the pion propagator simplify considerably. The contribution of the last but one term of (20) to the pion propagator breaks up upon working out the Dirac structure into the linear combination of a fermionic tadpole $\tilde{T}(m_q)$ and a bubble integral $\tilde{I}(p;m_q)$. Introducing the propagator

$$D_0(k) = \frac{i}{k^2 - m_q^2}, \quad (25)$$

these integrals are defined as

$$\tilde{T}(m_q) = \frac{1}{N_c}\sum_{i=1}^{N_c}\int_k D_0(k), \quad (26)$$

$$\tilde{I}(p;m_q) = \frac{1}{N_c}\sum_{i=1}^{N_c}\Big[-i\int_q D_0(q)D_0(q+p)\Big]. \quad (27)$$

In terms of these integrals which are evaluated in the Appendix between Eqs. (A11) and (A18) one obtains

$$0 = Nv\Big[m^2 + \frac{\lambda}{6}\Big(v^2 + \int_k G_\pi(k)\Big) - \frac{4g^2N_c}{\sqrt{N}}\tilde{T}(m_q) - \frac{h}{v}\Big] + \text{c.t.}, \quad (28)$$

$$iG_\pi^{-1}(k) = k^2 - m^2 - \frac{\lambda}{6}\Big(v^2 + \int_k G_\pi(k)\Big) + \frac{4g^2N_c}{\sqrt{N}}\tilde{T}(m_q) - \frac{2g^2N_c}{\sqrt{N}}k^2\tilde{I}(p;m_q) + \text{c.t.} \quad (29)$$

One can see that the Goldstone theorem is fulfilled, since using the EoS in the equation for the pion propagator one obtains $iG_\pi^{-1}(k=0) = -h/v$. This is only accidental because the Ward identity relating the inverse fermion propagator and the proper vertex $\Gamma_{\pi^a\psi\bar{\psi}} = \delta^3\Gamma/\delta\bar{\psi}\delta\psi\delta\pi^a$ [see e.g. Eq. (13.102) of [65]]

$$-\frac{i}{2}T_a\{\gamma_5, iG^{-1}(p)\} = v\sqrt{\frac{N}{2N_f}}\Gamma_{\pi^a\psi\bar{\psi}}(0,p,-p), \quad (30)$$

is satisfied only with tree-level propagators and vertices. The relation above is violated at any order of the perturbation theory in the large-N_f approximation, since in view of (24) the corrections to the inverse tree-level fermion propagator are of $\mathcal{O}(1)$, while the corrections to the tree-level $\pi - \psi - \bar{\psi}$ vertex are suppressed by $1/N$.

(2) A further approximation concerns the self-consistent pion propagator (29). In this work four approximations for G_π are considered: two local approximations and two nonlocal approximations obtained using an expansion in $1/\sqrt{N}$. In the local approximation one parametrizes the pion propagator as

$$G_{\pi,l}(p) = \frac{i}{p^2 - M^2}, \quad (31)$$

and uses this form in all equations. In the *first* variant M^2 is determined as a pole mass from $iG_{\pi,l}^{-1}(p_0^2 = M^2, \mathbf{p} = 0) = 0$ by the self-consistent gap equation arising from (29)

$$M^2 = m^2 + \frac{\lambda}{6}(v^2 + T_F(M)) - \frac{4g^2N_c}{\sqrt{N}}\tilde{T}_F(m_q) + \frac{2g^2N_c}{\sqrt{N}}M^2\tilde{I}_F(M,\mathbf{0};m_q). \quad (32)$$

In a *second* variant M^2 is determined from $M^2 = -iG_{\pi,l}^{-1}(p=0)$, when the gap equation becomes

$$M^2 = m^2 + \frac{\lambda}{6}(v^2 + T_F(M)) - \frac{4g^2N_c}{\sqrt{N}}\tilde{T}_F(m_q). \quad (33)$$

The subscript F denotes the finite part of the integrals defined in Eqs. (26) and (27), which are given explicitly in Eqs. (A13) and (A16)–(A18). In this way the finite parts of all vacuum pieces are contained in our equation. The importance of these terms for the thermodynamics of the PQM model was pointed out in [29]. In view of the EoS (28) the two definitions of M^2 coincide in the chiral limit $h = 0$, where for both variants one has $M^2 = 0$. We note that due to their self-consistent nature, when (32) or (33) is solved, a series containing all orders of $1/\sqrt{N}$ is in fact resummed.

The *third*, nonlocal variant of the pion equation is derived using an $1/\sqrt{N}$ expansion in the pion propagator (29) after exploiting the EoS (28). One obtains

$$G_\pi(p) = \frac{i}{p^2 - \frac{h}{v} - \frac{2g^2N_c}{\sqrt{N}} p^2 \tilde{I}_F(p; m_q)} = \frac{i}{p^2 - \frac{h}{v}} + \frac{2g^2N_c}{\sqrt{N}} \frac{ip^2 \tilde{I}_F(p; m_q)}{(p^2 - \frac{h}{v})^2} + \mathcal{O}\left(\frac{1}{N}\right). \quad (34)$$

With this form of the pion propagator the EoS reads

$$\frac{h}{v} = m^2 + \frac{\lambda}{6}(v^2 + T_F(M)) + \frac{2g^2N_c}{\sqrt{N}} J_F(M, m_q) - \frac{4g^2N_c}{\sqrt{N}} \tilde{T}_F(m_q), \quad (35)$$

where in this case $M^2 = h/v$ and we have introduced the integral

$$J(M, m_q) = -i \int_p G^2_{\pi,l}(p) p^2 \tilde{I}_F(p; m_q). \quad (36)$$

Solving this equation for v shows that this approximation still resums infinitely many orders in $1/\sqrt{N}$.

A *fourth* variant of G_π, which by a strict expansion in $1/\sqrt{N}$ will include terms of no higher order than $\mathcal{O}(1/\sqrt{N})$, can be obtained by expanding not only the nonlocal, momentum-dependent part of the self-energy in the pion propagator (29), but also its local part. This is explicitly constructed including counterterms in Sec. III, where a diagrammatic illustration of the approximation is also given. For this approximation, the pion propagator is given by Eqs. (42), (44), and (46), while the EoS is given in (53).

E. Parametrization

The mass parameter m^2, the couplings g, λ, the renormalization scale M_{0B}, the vacuum expectation value v_0, and the external field h, which vanishes in the chiral limit, are determined at $T = \mu_q = 0$ using some information from the sigma sector and the following physical quantities: the pion decay constant $f_\pi = 93$ MeV and its mass $m_\pi = 140$ MeV, and the constituent quark mass taken to be $M_q = m_N/3 = 313$ MeV. From the sigma sector we use the mass and the width of the sigma particle and the behavior of the spectral function. v_0 is determined from the matrix element of the axial vector current between the vacuum state and a one-pion state, which due to the rescaling of the vacuum expectation value by $\sqrt{N}$ gives $v_0 = f_\pi/2$. The value of the Yukawa coupling $g = 6.7$ is obtained by equating the tree-level fermion mass m_q with M_q. The parameters λ and M_{0B} are determined from the sigma propagator, as will be detailed below. Having determined them, in the chiral limit m^2 is fixed from the EoS, while in the case of the physical pion mass the remaining parameters m^2 and h are determined as follows. If the local approximation for the pion propagator is used m^2 is determined from the gap equation by requiring $M^2 = m_\pi^2$, and h is obtained from the EoS. When G_π is approximated using a large-N_f expansion h is fixed by requiring $h = m_\pi^2 v_0$, and m^2 is determined from the EoS.

Now we turn to the issue of fixing λ and M_{0B}. Using in (23) the tree-level fermion propagator together with the local approximation (31) for the pion propagator and also the equation of state (28), one obtains after working out the Dirac structure the following form for the sigma propagator:

$$iG_\sigma^{-1}(p) = p^2 - \frac{h}{v} - \frac{\lambda v^2}{3} \frac{1}{1 - \lambda I_F(p; M)/6} + \frac{2g^2N_c}{\sqrt{N}} (4m_q^2 - p^2) \tilde{I}_F(p; m_q). \quad (37)$$

The integral $I_F(p; M)$, obtained using the local approximation (31) for the pion propagator with $M^2 = m_\pi^2$, can be found in Eqs. (10) and (11) of Ref. [59] with M_0 replaced by M_{0B}, while $\tilde{I}_F(p; m_q)$ is given in Eqs. (A16)–(A18).

Both in the chiral limit $M = 0$ and for $M = m_\pi$ the self-energy has along the positive real axis of the complex p_0 plane two cuts above the thresholds of the pion and fermion bubble integrals, which start at $p^2 = 4M^2$ and $p^2 = 4m_q^2$, respectively. Above these thresholds the respective pion and fermion bubble integrals have nonvanishing imaginary parts. We search for poles of the sigma propagator analytically continued between the two cuts to the second Riemann sheet in the form $iG_\sigma^{-1}(p_0 = \kappa e^{-i\phi}, \mathbf{p} = 0) = 0$. The pole is parametrized as $p_0 = M_\sigma - i\Gamma_\sigma/2$, with the real and imaginary parts corresponding to the mass and the half-width of the sigma particle. The solution for M_σ and Γ_σ is shown in Fig. 1 both in the chiral limit ($h = m_\pi = 0$) and for the $h \neq 0$ case. Similar to the case of the $O(N)$ model studied in Ref. [59], in the chiral limit the value of M_σ is a little smaller and the value of Γ_σ larger than in the $h \neq 0$ case. Comparing Fig. 1 with Fig. 2 of Ref. [59] obtained in the $O(N)$ model, that is without fermions, the $M_\sigma(\lambda)$ curve moved slightly upward, but the $\Gamma_\sigma(\lambda)$ curve moved significantly downward, which means that in the present case the phenomenologically expected value [66] $M_\sigma/\Gamma_\sigma \sim 1$ cannot be achieved for any value of the coupling λ. Another difference is that for low values of λ there are

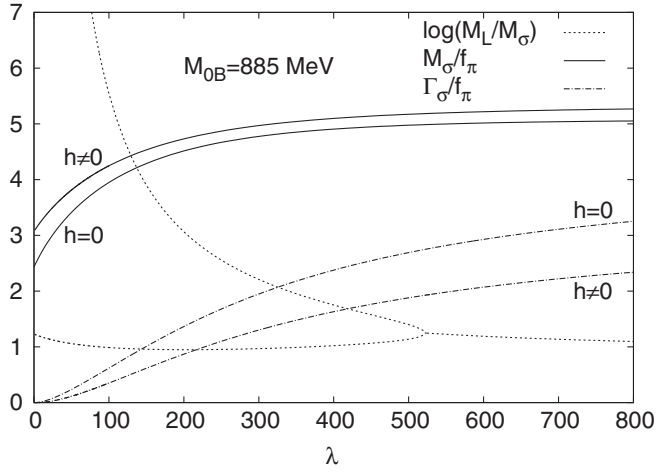

FIG. 1. The λ dependence of the real and imaginary parts of the complex sigma pole $p_0 = M_\sigma - i\Gamma_\sigma/2$ and of the Landau ghost M_L in the chiral limit and for the physical pion mass. The upper curve for M_σ and the lower one for Γ_σ represent the case of the physical pion mass, as indicated on the plot. M_L is shown only in this case, for in the chiral limit there is very little difference.

two poles of G_σ on the negative imaginary axis in contrast to only one such pole in the $O(N)$ model. These poles approach each other as λ increases and after they collide at a given value of λ there are two complex poles at higher λ, one with positive and one with negative real part. The imaginary part of the complex pole having positive real part is shown in Fig. 1 for the renormalization scale $M_{0B} =$ 885 MeV. As explained in the study done in the chiral limit in [40] for lower values of the renormalization scale the scale M_L of the lower Landau ghost on the imaginary axis comes even closer to M_σ and as a result the spectral function of the sigma is heavily distorted. In order to avoid this and based on the ratio of M_σ/Γ_σ we have chosen $\lambda =$ 400 and $M_{0B} = 885$ MeV. For these values $M_\sigma =$ 456 MeV and $\Gamma_\sigma = 221$ MeV in the chiral case, while $M_\sigma = 474$ MeV and $\Gamma_\sigma = 152$ MeV for the case of a physical pion mass. These values are used throughout Sec. IV also in the case when the pion propagator is expanded in $1/\sqrt{N}$, that is in the third and fourth variants of G_π discussed in Sec. II D.

III. RENORMALIZATION

The lesson one can learn from the successful renormalization in 2PI [67–71] or large-N [64,72,73] approximations is that, due to the systematic nature of these expansions, the counterterms can be obtained by analyzing the structure of the equations. In these cases there is no need for an order-by-order detailed study of the counterterm diagrams which becomes rather complicated due to the proliferation of the diagrams. If one uses some *ad hoc* approximation which spoils the self-consistent nature of the propagator equations or is not systematic, then one loses the possibility to explicitly or uniquely determine the counterterms from the equations.

In this section we discuss the renormalization of the model in the case of a strict $1/\sqrt{N}$ expansion in the pion propagator and the equation of state. This expansion is not entirely consistent because as mentioned in Sec. II D we use for simplicity tree-level fermion propagators despite the fact that this expansion produces $\mathcal{O}(1)$ corrections in the fermion propagator (24) which all have to be resummed. We will see that as a consequence of this approximation the best one can achieve is to determine the counterterms to some order in the Yukawa coupling. It will turn out that the order depends on the equation and the type of subdivergence we are looking at.

The counterterm functional needed to renormalize the pion propagator and the equation of state reads

$$\begin{aligned}\Omega_{\mathrm{c.t.}}[G_\pi, v] = &\frac{N}{2}\delta m_0^2 v^2 + \frac{N}{24}\delta\lambda_4 v^4 \\ &+ \frac{N-1}{2}\left(\delta m_2^2 + \frac{\delta\lambda_2}{6}v^2\right)\int_k G_\pi(k) \\ &+ (N-1)\frac{\delta\lambda_0}{24}\left[\int_k G_\pi(k)\right]^2 \\ &- (N-1)\frac{\delta Z}{2}\int_k k^2 G_\pi(k). \end{aligned} \tag{38}$$

Compared to the counterterm functional used in Eq. (48) of [64] to renormalize the stationary equations of the $O(N)$ model the only difference in (38) is the appearance of the term containing the wave-function renormalization counterterm δZ. This is needed to remove the momentum-dependent divergence of the fermionic contribution to the pion propagator (29) rewritten as

$$iG_\pi^{-1}(k) = (1 + \delta Z)k^2 - M^2 - \frac{2g^2 N_c}{\sqrt{N}} k^2 \tilde{I}(k; m_q). \tag{39}$$

The local part M^2 containing the remaining counterterms reads

$$\begin{aligned} M^2 = &\, m^2 + \delta m_2^2 + \frac{\lambda + \delta\lambda_2}{6} v^2 + \frac{\lambda + \delta\lambda_0}{6}\int_p G_\pi(p) \\ &- \frac{4g^2 N_c}{\sqrt{N}}\tilde{T}(m_q). \end{aligned} \tag{40}$$

Using in (39) the notation introduced in (A15) one can readily determine δZ:

$$\delta Z = \frac{2g^2 N_c}{\sqrt{N}}\tilde{I}_{\mathrm{div}}(k; m_q) = \frac{2g^2 N_c}{\sqrt{N}} T_d^{(0)}. \tag{41}$$

Separating the LO and NLO contributions in the local part given in (40) by writing $M^2 = M^2_{\mathrm{LO}} + M^2_{\mathrm{NLO}}/\sqrt{N}$, an expansion in powers of $1/\sqrt{N}$ in the pion propagator (39) gives

$$G_\pi(p) = G_{\rm LO}(p) - i\frac{G^2_{\rm LO}(p)}{\sqrt{N}}[M^2_{\rm NLO} - 2N_c g^2 p^2 \tilde{I}_F(p;m_q)] + \mathcal{O}\left(\frac{1}{N}\right), \tag{42}$$

where $G_{\rm LO}(p) = i/(p^2 - M^2_{\rm LO})$. The counterterms are also written as the sum of LO and NLO contributions $\delta m_i^2 = \delta m_i^{2(0)} + \delta m_i^{2(1)}/\sqrt{N}$, $\delta\lambda_i = \delta\lambda_i^{(0)} + \delta\lambda_i^{(1)}/\sqrt{N}$ and used together with (42) in (40) to obtain the equations for the LO and NLO local parts

$$M^2_{\rm LO} = m^2 + \delta m_2^{2(0)} + \frac{\lambda + \delta\lambda_2^{(0)}}{6}\upsilon^2 + \frac{\lambda + \delta\lambda_0^{(0)}}{6}T(M_{\rm LO}), \tag{43a}$$

$$M^2_{\rm NLO}\left[\frac{1}{\lambda_B^{(0)}} - \frac{I(0;M_{\rm LO})}{6}\right] = \frac{1}{\lambda_B^{(0)}}\left[\delta m_2^{2(1)} + \frac{\delta\lambda_2^{(1)}}{6}\upsilon^2 + \frac{\delta\lambda_0^{(1)}}{6}T(M_{\rm LO})\right] - \frac{4g^2}{\lambda_B^{(0)}}N_c\tilde{T}(m_q) + \frac{2g^2}{6}N_c J(M_{\rm LO}, m_q), \tag{43b}$$

where we divided the second equation by $\lambda_B^{(0)} = \lambda + \delta\lambda_0^{(0)}$ and used the integral introduced in (36) with $G_{\pi,l}$ replaced by $G_{\rm LO}$.

Compared to the perturbative renormalization of the fermionic trace-log contribution to the effective potential performed in [31], the difficulty here is that, due to the self-consistent nature of the pion propagator, an infinite series of coupling counterterms of the mesonic part, that is $\delta\lambda_0$, $\delta\lambda_2$, δm_0^2, and δm_2^2 has to be determined to $\mathcal{O}(\sqrt{N})$ of the large-N expansion. In order to achieve this we apply the method developed in Refs. [60,71,73]. The method for determining the counterterms appearing in a particular equation resides in the separation of the divergent part of the integrals contained by the equation. This is obtained by expanding the propagators around an appropriately defined auxiliary propagator (see Appendix A of [71]). Then, the finite part of the integrals is used to write down a finite equation, which, when subtracted from the original equation, provides a relation between counterterms and divergences. This relation still involves the vacuum expectation value υ and the finite part of some integrals, e.g. T_F, the finite part of the pion tadpole. Requiring as in [73] the vanishing of the coefficient of υ^2 and T_F (cancellation of subdivergences) one obtains the coupling counterterms, while the remaining part of the relation mentioned above gives the mass counterterm (cancellation of the overall divergence).

To apply the above method to Eq. (43a) for $M^2_{\rm LO}$, which is the gap equation of the $O(N)$ model at leading order of the large-N approximation, one uses the expression of the pion tadpole given in (A6) in terms of finite and divergent pieces. Retaining in (43a) the finite part of the tadpole one obtains the LO finite gap equation

$$M^2_{\rm LO} = m^2 + \frac{\lambda}{6}[\upsilon^2 + T_F(M_{\rm LO})]. \tag{44}$$

Subtracting this from (43a) one requires the vanishing of the coefficient of υ^2 and $T_F(M_{\rm LO})$ in the resulting equation. This determines the LO coupling counterterms

$$\delta\lambda_2^{(0)} = \delta\lambda_0^{(0)} = -\frac{\lambda^2}{6}\frac{T_d^{(0)}}{1 + \lambda T_d^{(0)}/6}, \tag{45}$$

while requiring the cancellation of the remaining overall divergence determines the LO mass counterterm $\delta m_2^{2(0)} = -(\lambda + \delta\lambda_0^{(0)})[T_d^{(2)} + [M^2 - M_0^2]T_d^{(0)}]/2$.

The determination of the counterterms in the equation for the NLO local part in the pion propagator parallels to some extent the analysis of the NLO divergences in the $O(N)$ model discussed in Sec. VI B of [64]. One observes that since $I_{\rm div}(0;M_{\rm LO}) = T_d^{(0)}$, in view of (45) the left-hand side of (43b) is finite and it actually enters the finite equation for $M^2_{\rm NLO}$

$$M^2_{\rm NLO}\left[\frac{1}{\lambda} - \frac{I_F(0;M_{\rm LO})}{6}\right] = -\frac{4g^2}{\lambda}N_c\tilde{T}_F(m_q) + \frac{2g^2}{6}N_c J_F(M_{\rm LO}, m_q). \tag{46}$$

Subtracting (46) from (43b) the following relation between divergences and counterterms is obtained:

$$0 = \frac{1}{\lambda_B^{(0)}}\left[\delta m_2^{2(1)} + \frac{\delta\lambda_2^{(1)}}{6}\upsilon^2 + \frac{\delta\lambda_0^{(1)}}{6}T(M_{\rm LO}) - 4g^2\tilde{T}_{\rm div}(m_q)\right] - 4g^2N_c\frac{T_d^{(0)}}{6}\tilde{T}_F(m_q) + \frac{2g^2}{6}N_c J_{\rm div}(M_{\rm LO}, m_q). \tag{47}$$

Then we use the expression of $J_{\rm div}(M_{\rm LO}, m_q)$ given in (A28) in terms of $M_{\rm LO}$, m_q^2, and $\tilde{T}(m_q)$ in which one substitutes for $M_{\rm LO}$ its expression from (44). The terms proportional to $\tilde{T}_F(m_q)$ cancel. The overall divergences determine the form of $\delta m_2^{2(1)}$. The remaining terms proportional to υ^2 and $T_F(M_{\rm LO})$ can be grouped as

$$\cdots + \frac{\upsilon^2}{6}\left\{\delta\lambda_2^{(1)} + \frac{\lambda\delta\lambda_0^{(1)}}{6}T_d^{(0)} + \frac{2g^2}{3}N_c\lambda\lambda_B^{(0)}T_d^{(I)} + 4g^4N_c[\lambda_B^{(0)}(T_d^{(I)} + (T_d^{(0)})^2) - 6g^2T_d^{(0)}]\right\} + \frac{T_F(M_{\rm LO})}{6}\left[\delta\lambda_0^{(1)} + \frac{\lambda\delta\lambda_0^{(1)}}{6}T_d^{(0)} + \frac{2g^2}{3}N_c\lambda\lambda_B^{(0)}T_d^{(I)}\right] = 0. \tag{48}$$

Requiring the vanishing of the coefficient of υ^2 and $T_F(M_{\rm LO})$ determines the NLO coupling counterterms

$\delta\lambda_2^{(1)}$ and $\delta\lambda_0^{(1)}$. One can see that these counterterms agree at $\mathcal{O}(g^2)$ but differ at $\mathcal{O}(g^4)$.

A completely similar analysis performed on the EoS

$$m^2 + \delta m_0^2 + \frac{\lambda + \delta\lambda_4}{6}v^2 + \frac{\lambda + \delta\lambda_2}{6}\int_k G_\pi(k) - \frac{4g^2N_c}{\sqrt{N}}\tilde{T}(m_q) = \frac{h}{v} \tag{49}$$

gives an equation analogous in form and meaning to (48)

$$\cdots + \frac{v^2}{6}\left\{\delta\lambda_4^{(1)} + \frac{\lambda\delta\lambda_2^{(1)}}{6}T_d^{(0)} + \frac{2g^2}{3}N_c\lambda\lambda_B^{(0)}T_d^{(I)} + 4g^4N_c[\lambda_B^{(0)}(T_d^{(I)} + (T_d^{(0)})^2) - 6g^2T_d^{(0)}]\right\} + \frac{T_F(M_{\rm LO})}{6} \times\left[\delta\lambda_2^{(1)} + \frac{\lambda\delta\lambda_2^{(1)}}{6}T_d^{(0)} + \frac{2g^2}{3}N_c\lambda(\lambda + \delta\lambda_0^{(0)})T_d^{(I)}\right] = 0. \tag{50}$$

From this equation one can see that the NLO coupling counterterms $\delta\lambda_2^{(1)}$ and $\delta\lambda_4^{(1)}$ agree at $\mathcal{O}(g^2)$ but differ at $\mathcal{O}(g^4)$. Moreover, one sees that $\delta\lambda_2^{(1)}$ determined from the requirement to cancel the coefficient of v^2 in (50) differs at $\mathcal{O}(g^4)$ from $\delta\lambda_2^{(1)}$ needed to cancel the coefficient of $T_F(M_{\rm LO})$ in (50). These requirements give the same expression for the counterterm only at $\mathcal{O}(g^2)$.

The above feature is a consequence of the fact that by keeping the fermions unresummed one does not take into account all the diagrams which are of the same order in the large-N_f expansion. It does not necessarily mean that the approximation we use is unrenormalizable. Rather we suggest the interpretation that the approximation is such that different subseries of the counterterms are needed to cancel the subdivergences of different equations. Although we have a method to determine the counterterms in each equation, corrections are to be expected starting at $\mathcal{O}(g^4)$. If one traces back the origin of the term proportional to $T_F(M_{\rm LO})$ in (48) one finds that it comes from the expression (44) for $M^2_{\rm LO}$ used in the divergent contribution $J_{\rm div}(M_{\rm LO}, m_q)$ as given by (A28). In turn, the integral $J(M_{\rm LO}, m_q)$ defined in (36) is generated through the expansion (42) by the one-loop fermion bubble contribution to the pion self-energy. But, when the first correction to the fermion propagator is included, then we have to take into account in the square bracket of the expanded pion propagator (42) the contribution of the two-loop self-energy

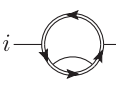

$$= \frac{g^4N_c}{\sqrt{N}}\Sigma_2(p; M_{\rm LO}, m_q). \tag{51}$$

This will generate in the equation for $M^2_{\rm NLO}$ an integral similar to $J(M_{\rm LO}, m_q)$

$$g^4K(M_{\rm LO}, m_q) = -ig^4\int_p G^2_{\rm LO}(p)\Sigma_2(p; M_{\rm LO}, m_q), \tag{52}$$

which is expected to have a divergence proportional to $T_F(M_{\rm LO})$. This divergence would result in $\mathcal{O}(g^4)$ corrections in the $\delta\lambda_0^{(1)}$ counterterm as determined from (48). Therefore, it is expected that with a resummed fermion propagator, as required by the large-N_f resummation, the determined counterterms will eventually agree in all equations. It is rather nontrivial to check this conjecture, even at the two-loop level, because the reduction of the two-loop integral in (51) performed with the method of [74] produces more than a dozen scalar integrals and their contribution should be analyzed in (52). We have only checked that at the two-loop level the Goldstone theorem is indeed violated as mentioned in Sec. II D, based on the violation of the Ward identity (30).

Before closing this section we give in Fig. 2 the diagrammatic illustration of the equation of state obtained by a strict expansion to first order in $1/\sqrt{N}$ of the self-consistent pion propagator. This corresponds to the fourth approximation to the pion propagator discussed in Sec. II D. Because we do not draw the counterterm diagrams, we actually obtain the unrenormalized EoS which reads

$$M^2_{\rm LO} + \frac{1}{\sqrt{N}}M^2_{\rm NLO} = \frac{h}{v}, \tag{53a}$$

$$M^2_{\rm LO} = m^2 + \frac{\lambda}{6}[v^2 + T(M_{\rm LO})], \tag{53b}$$

$$M^2_{\rm NLO} = \frac{4g^2N_c}{1 - \frac{\lambda}{6}I(0; M_{\rm LO})}\left[-\tilde{T}(m_q) + \frac{\lambda}{12}J(M_{\rm LO}, m_q)\right], \tag{53c}$$

where $I(0; M_{\rm LO}) = dT(M)/(dM^2)$, with $T(M)$ defined in (A6). The first set of diagrams are the $\mathcal{O}(\sqrt{N})$ superdaisy diagrams made of pions with tree-level propagators. Their resummation is clearly provided by (53b), as one can check iteratively. The second set of diagrams is $\mathcal{O}(1)$ and contains only a single insertion of a fermion bubble. Using Feynman rules, one can readily check that when the chain of pion bubbles is resummed one obtains

$$-\frac{\lambda g^2 v/6}{1 - \frac{\lambda}{6}I(0; M_{\rm LO})}\int_k G^2_{\rm LO}(k)\int_p {\rm tr}_{c,D}[\gamma_5 D(p)\gamma_5 D(k+p)] = \frac{4N_c\lambda g^2 v/6}{1 - \frac{\lambda}{6}I(0; M_{\rm LO})}\left[-I(0; M_{\rm LO})\tilde{T}(m_q) + \frac{1}{2}J(M_{\rm LO}, m_q)\right]. \tag{54}$$

Adding this to the fermion tadpole and dividing by v one obtains the expression of $M^2_{\rm NLO}$ given in (53c). The finite version of the EoS (53) is obtained by replacing the integrals by their finite parts taken from the Appendix.

If one would try to use the method described in this section to renormalize the EoS (28) using the local pion propagator (31) with a mass determined from the gap equation (32), one would encounter a subdivergence proportional to $\tilde{I}_F(M, \mathbf{0}; m_q)$ which is not canceled. This is an artifact of the local approximation used and a

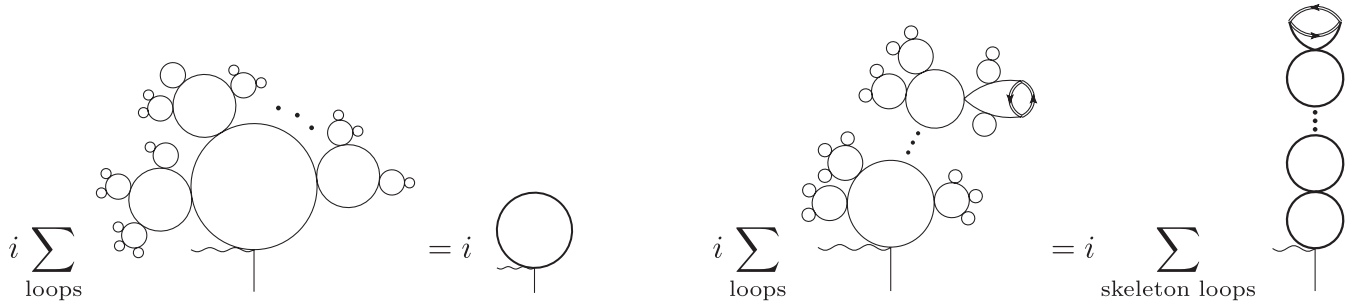

FIG. 2. Leading order and next-to-leading order diagrams resummed in the equation of state obtained by expanding the self-consistent pion propagator to first order in $1/\sqrt{N}$. The tree-level pion and fermion propagators are denoted by thin and double lines, while the thick line represents the resummed LO pion propagator.

self-consistent treatment of the propagator would unfold this into renormalizable pieces as happened already when the propagator was expanded consistently in $1/\sqrt{N}$. As we have seen, in this case only subdivergences proportional with v^2 and $\tilde{T}_F(m_q)$ appeared. As a consequence, we will not attempt to explicitly construct the counterterms when using other approximate forms of the pion propagator given in Sec. II D. Fortunately, in these cases, since the propagators are of a tree-level form, the finite part of the integrals can be easily determined and we assume that in a given equation the subtraction of the infinite part of an integral can be achieved by a corresponding subset of the full series of counterterm diagrams.

IV. THE $\mu_q - T$ PHASE DIAGRAM

The thermodynamics is determined by solving the field equations, i.e. the EoS (28) and the equations giving the dependence on T and μ_q of the two real mean fields Φ and $\bar{\Phi}$. When the full fermion propagator is replaced by the tree-level one, one has in view of Eqs. (A1)–(A5) and (A35)–(A37)

$$\frac{dU(\Phi,\bar{\Phi})}{d\Phi} - 2N_c\sqrt{N}\int\frac{d^3\mathbf{k}}{(2\pi)^3}\frac{k^2}{3E_k}\left(\frac{d\tilde{f}^+_\Phi(E_k)}{d\Phi}+\frac{d\tilde{f}^-_{\bar{\Phi}}(E_k)}{d\Phi}\right) + g^2\sqrt{N}N_c\Big[2(\tilde{T}^0_F(m_q)-T_F(M))\frac{d\tilde{T}^\beta(m_q)}{d\Phi}+\frac{d\tilde{T}^{\beta,2}_2(m_q)}{d\Phi} - M^2\left(\frac{dS^{\beta,1}(M,m_q)}{d\Phi}+\frac{dS^{\beta,2}(M,m_q)}{d\Phi}\right)\Big] = 0, \tag{55}$$

where $E_k = (\mathbf{k}^2 + m_q^2)^{1/2}$ and M satisfies either one of the gap equations (32) and (33), or (43a), or the relation $M^2 = h/v$. The other equation is similar to (55), the only difference is that the derivative is taken with respect to $\bar{\Phi}$. The integral in (55) is the contribution of the fermionic trace-log integral defined in Eq. (A1), while the term proportional with g^2 is the contribution of the quark-pion two-loop integral in (20) given in Eq. (A35). When solving the field equations for Φ and $\bar{\Phi}$, we disregard for simplicity the contribution of the setting sun and keep only the one-loop contribution coming from the fermionic trace log. The complete equation (55) is solved only in one case (see the last row of Table II) in order to estimate the error made by neglecting this term in all the other cases. To solve the field equations we use for the pion propagator a given approximation described in Sec. II D as will be specified below.

The tricritical point (TCP) and the critical end point (CEP) are identified as the points along the chiral phase transition line of the $\mu_q - T$ phase diagram where a first order phase transition turns with decreasing μ_q into a second order or crossover transition, respectively. In case of a crossover, the temperature T_χ of the chiral transition is defined as the value where the derivative dv/dT has a minimum [inflection point of $v(T)$], while the temperature T_d of the deconfinement transition is obtained as the location of the maximum in $d\Phi/dT$. The transition point in the case of a first order phase transition is estimated by the inflection point located between the turning points of the multivalued curve $v(\mu_q)$ obtained for a given constant temperature. Although the precise definition of the 1st order transition point is given by that value of the intensive parameter for which the two minima of the effective potential are degenerate, we adopt the definition based on the inflection point, which is also commonly used in the literature, because we are not computing the effective potential, but only its derivatives with respect to the fields and propagators.

A. Phase transition in the chiral limit

In the chiral limit we solve the EoS (28) using only the local approximation to the pion propagator (31) with $M^2 = 0$. The critical temperature of the chiral transition T_χ and the pseudocritical temperature T_d of the deconfinement transition at vanishing chemical potential, and the location of the TCP are summarized in Table I for various forms of the Polyakov-loop potential. On one hand, one can see that with the inclusion of the Polyakov loop $T_\chi(\mu_q = 0)$ and T_{TCP} increase significantly compared with the values obtained earlier in [40] without the Polyakov loop. On the other hand, in all cases, the inclusion of the Polyakov

TABLE I. The critical temperature T_χ of the chiral transition and the pseudocritical temperature T_d of the deconfinement transition at $\mu_q = 0$, and the location of the TCP in units of MeV obtained in the chiral limit without the Polyakov loop (first row) and with the inclusion of the Polyakov loop using various effective potentials summarized in Sec. II B.

$U(\Phi, \bar{\Phi})$	T_0	$T_\chi(\mu_q = 0)$	$T_d(\mu_q = 0)$	$T_{\rm TCP}$	$\mu_q^{\rm TCP}$
⋯	⋯	139.0	⋯	60.7	277.0
poly	270	185.6	229.0	104.5	261.8
poly	208	168.2	176.5	96.2	263.4
log	270	191.4	209.0	109.4	261.2
log	208	167.6	162.4	102.6	261.2
log	$T_0(\mu_q)$	167.9	162.8	84.3	266.9
Fuku	⋯	176.5	193.0	99.8	262.2

loop has little effect on the value of $\mu_q^{\rm TCP}$. The increase in $T_\chi(\mu_q = 0)$ obtained with the inclusion of the Polyakov-loop effective potential is basically determined by the value of its parameter T_0, while the value of $T_{\rm TCP}$ shows no significant variation among different cases having the same value of T_0. One can also see that, as explained in [56], the use of the polynomial and logarithmic effective potentials for the Polyakov loop, that is (5) and (7), drags the value of $T_\chi(\mu_q = 0)$ closer to the value of the parameter T_0 than the use of $U_{\rm Fuku}(\Phi, \bar{\Phi})$ given in (9). In this latter case one obtains the smallest value for $T_{\rm TCP}$.

For $T_0 = 270$ MeV the deconfinement transition line in the $\mu_q - T$ phase diagram is above the chiral transition line in all three variants of the effective potential for the Polyakov loop. This is illustrated in the left panel of Fig. 3 in case of the polynomial effective potential, where the chiral phase diagram is compared to the one obtained without including the Polyakov loop. When the logarithmic effective potential $U_{\log}(\Phi, \bar{\Phi})$ is used either with a constant $T_0 = 208$ MeV or with the μ_q-dependent T_0 proposed in [27] one finds $T_d < T_\chi$ at $\mu_q = 0$, but at a given value of the chemical potential the deconfinement transition line crosses the chiral transition line and remains above it for higher values of μ_q. This is shown in the right panel of Fig. 3, where the deconfinement transition line is obtained from the inflection point of $\Phi(T)$. The transition line obtained from the inflection point of $\bar{\Phi}(T)$ is practically indistinguishable from the line shown in the figure. One can see that in contrast to the case of constant T_0, where basically the deconfinement transition line is not affected by the increase of μ_q, with a μ_q-dependent T_0 the deconfinement transition line strongly bends, staying close to the chiral line. The two lines cross just above the TCP.

The lowering of the deconfinement transition in the case when $T_0(\mu_q)$ is used and as a result the shrinking of the so-called quarkyonic phase was already observed in Ref. [17]. As distinguished from the mesonic phase which is confined and has zero quark number density and the

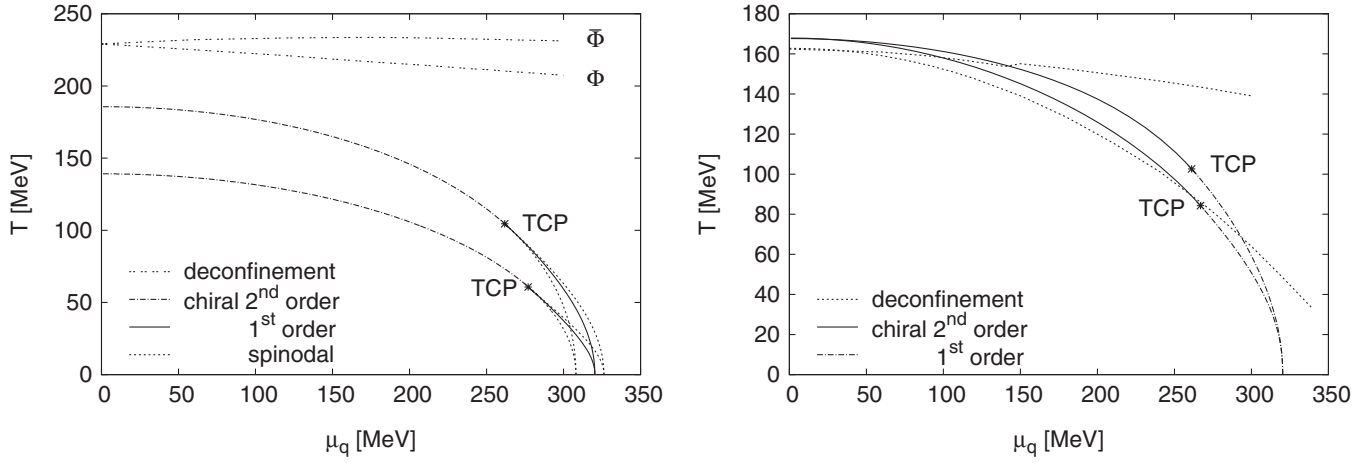

FIG. 3. Left panel: Phase diagrams obtained in the chiral limit without and with the inclusion of the Polyakov loop. The latter has higher $T_{\rm TCP}$ and was obtained using $U_{\rm poly}(\Phi, \bar{\Phi})$ with $T_0 = 270$ MeV. Shown are the location of the inflection points of $\Phi(T)$ and $\bar{\Phi}(T)$. Right panel: Chiral and deconfinement phase transitions obtained for $U_{\log}(\Phi, \bar{\Phi})$ with $T_0 = 208$ MeV (upper curves) and with $T_0(\mu_q)$ (lower curves). The deconfinement transition line is obtained from the inflection point of $\Phi(T)$.

deconfined phase which has finite quark number density, the quarkyonic phase is a confining state made of quarks and is characterized by a high quark number density and baryonic (three-quark state) thermal excitations. Based on the fact that in the PNJL model the quantity measuring the quark content inside thermally excited particles carrying baryon number shows a pronounced change along the chiral phase transition line, the region of the $\mu_q - T$ plane for which $T_\chi < T < T_d$ was identified in [56] with the quarkyonic phase. The first numerical evidence from lattice QCD for the existence of a phase which is neither the hadronic nor the deconfined phase and is characterized by a high value of the quark number density was given in [75]. This could be a candidate for the quarkyonic phase. Further evidence for such a state was reported also in [76] within the strong-coupling expansion of the lattice QCD.

Comparing our results on the phase diagram to those obtained in the chiral limit of the PNJL model one can notice differences of both qualitative and quantitative nature. In the nonlocal PNJL model of Ref. [24] the deconfinement phase transition line starts at $\mu_q = 0$ below the chiral transition line both for a polynomial and a logarithmic Polyakov-loop effective potential with $T_0 = 270$ MeV, so that the two transition lines cross at finite μ_q. In our case this happens only for the logarithmic potential with $T_0 = 208$ MeV, as can be seen in Fig. 3. In [19,24] the values of $T_\chi(\mu_q = 0)$ and $T_{\rm TCP}$ are much larger than in our case, while the value of $\mu_q^{\rm TCP}$ is similar to ours.

B. Phase transition in the case of the physical pion mass

In the case of the physical pion mass we solve the EoS (28) using each one of the four approximations to the pion propagator introduced in Sec. II D. Within the approximation corresponding to a strict expansion in $1/\sqrt{N}$ of the pion propagator and of the EoS discussed in detail in Sec. III there is no CEP in the $\mu_q - T$ phase diagram within a range $0 < \mu_q < 500$ MeV. Without inclusion of the Polyakov loop the transition at $\mu_q = 0$ is a very weak crossover characterized by a large value of the width at half maximum of $-dv/dT$, $\Gamma_\chi \sim 100$ MeV. Including the Polyakov loop, although the width at half maximum of $-dv/dT$ decreases by a factor of 2 compared to the case without the Polyakov loop, the transition remains a crossover for $\mu_q < 500$ MeV. This means that as a result of resumming in the pion propagator $\mathcal{O}(1/\sqrt{N})$ fermionic fluctuations, while keeping the fermion propagator unresummed, the crossover transition at $\mu_q = 0$ softens and increasing μ_q cannot turn the phase transition into a first order one. For the other three approximations, which all resum infinitely many orders in $1/\sqrt{N}$, the phase transition

TABLE II. The pseudocritical temperatures T_χ and T_d of the chiral and deconfinement transitions, the half width at half maximum Γ_χ of $-dv/dT$ at $\mu_q = 0$ (in the cases marked with *, due to an asymmetric shape of $-dv/dT$ the full width is given) and the location of the CEP in units of MeV obtained in various approximations for the pion propagator without and with the inclusion of the Polyakov loop. The two local approximations are defined by (32) and (33), respectively. The large-N approximation is defined by (34) and (35). Only for the result in the last row the contribution of the setting sun was kept in (55).

$U(\Phi, \bar{\Phi})$	T_0	$G_\pi(p)$	$T_\chi(\mu_q = 0)$	$T_d(\mu_q = 0)$	Γ_χ	$T_{\rm CEP}$	$\mu_q^{\rm CEP}$
...	...	local, pole	152.8	...	37.6	14.4	327.1
...	...	local, $p = 0$	158.2	...	41.5	12.1	329.1
...	...	large-N	158.6	...	40.7	13.5	328.6
poly	270	local, pole	205.6	226.8	25.6	37.8	326.9
poly	208	local, pole	180.6	175.0	19.8	35.3	326.7
poly	270	local, $p = 0$	211.4	217.8	27.3	32.4	329.0
poly	208	local, $p = 0$	184.6	176.7	22.7	30.1	328.9
poly	270	large-N	212.5	217.4	28.3	32.9	328.8
poly	208	large-N	184.6	176.8	22.3	30.6	328.8
log	270	local, pole	207.2	207.7	12.3	39.3	327.0
log	208	local, pole	168.0	167.0	*30.3	37.9	326.9
log	270	local, $p = 0$	209.8	209.3	12.1	33.9	329.1
log	208	local, $p = 0$	168.5	167.0	*42.8	32.7	329.0
log	$T_0(\mu_q)$	local, $p = 0$	168.9	167.4	*42.5	25.7	328.7
log	270	large-N	209.7	209.3	12.0	34.5	329.0
log	208	large-N	168.5	167.1	*43.0	33.0	328.9
Fuku	...	local, pole	191.0	188.7	19.8	36.2	326.8
Fuku	...	local, $p = 0$	195.3	191.2	21.2	31.2	328.9
Fuku	...	large-N	195.2	191.3	21.2	31.8	328.8
poly	208	large-N, full	188.1	183.1	21.4	32.2	329.0

turns with increasing μ_q from a crossover type into a first order transition and in consequence there is a CEP in the $\mu_q - T$ phase diagram. For these cases the result is summarized in Table II for various forms of the Polyakov-loop potential reviewed in Sec. II B.

In the cases studied in Table II increasing μ_q drives at $T = 0$ the restoration of chiral symmetry via a first order transition at some value $\mu_q^c > M_q$. Increasing the temperature μ_q^c decreases and the first order chiral restoration becomes a crossover at a much lower temperature $T_{\rm CEP}$ than in the chiral case. The inclusion of the Polyakov loop increases significantly the value of $T_{\rm CEP}$, but as in the chiral case it has little effect on the value of $\mu_q^{\rm CEP}$. One can see that neither the choice of the effective potential for the Polyakov loop nor the value of T_0 has a significant effect on the value of $\mu_q^{\rm CEP}$. Some variation can be observed among the values of $\mu_q^{\rm CEP}$ obtained using different approximations for the pion propagator. The result in the last row was obtained by keeping in the field equation of the Polyakov loop (55) and its conjugate the contribution of the setting-sun diagram, while in all other cases only the contribution of the fermionic trace log was kept. Comparing the result in the last row with that of the last row obtained using the polynomial Polyakov-loop potential, one can see that the error we make by neglecting the setting-sun contribution in all other cases is fairly small.

The values of T_χ and T_d at $\mu_q = 0$ are mostly influenced by the choice of the Polyakov effective potential and the value of T_0: they decrease with the decrease of T_0 and by using the logarithmic potential instead of the polynomial one. Using the polynomial potential with $T_0 = 270$ MeV the confinement transition line in the $\mu_q - T$ plane is above the chiral transition line. This can be seen in the left panel of Fig. 4 where the phase diagram is compared with the one obtained without the inclusion of the Polyakov loop. As in the chiral case, when a logarithmic potential is used with either a fixed value $T_0 = 208$ MeV or with a μ_q-dependent T_0, the deconfinement transition line starts at $\mu_q = 0$ below the chiral one and the two lines cross at some higher value of μ_q. This can be seen in the right panel of Fig. 4. When $T_0(\mu_q)$ is used the two lines go together until they cross each other just above the location of the CEP. This μ_q-dependent T_0 gives the lowest value of $T_{\rm CEP}$, similar to the results reported in [21,32]. Because of the much lower value of the $T_{\rm CEP}$ the shrinking of the quarkyonic phase is more pronounced than in the chiral case, as the deconfinement transition line approaches the μ_q axis. This is even more the case here, with a physical pion mass, since the deconfinement transition is a crossover and as such it happens in a relatively large temperature interval. However, the quarkyonic phase does not vanish completely as happens in [32], where quantum fluctuations are included using functional renormalization group methods.

By studying the derivatives of the $v(T)$ and $\Phi(T)$ curves one observes in panels (a) and (e) of Fig. 5 that at low μ_q it is the Polyakov loop which plays the driving role in the transition: for $\mu_q = 0$ the dv/dT is much wider and has a small peak in the temperature range where $\Phi(T)$ shows a pronounced variation. This happens only for very low values of μ_q, as in the region of μ_q where the deconfinement transition line is a little bit further below the chiral transition line than for $\mu_q = 0$, such a driving role cannot be identified. For values of μ_q where the two transition lines cross and also in the region where the chiral transition line is below the deconfinement one can see the influence

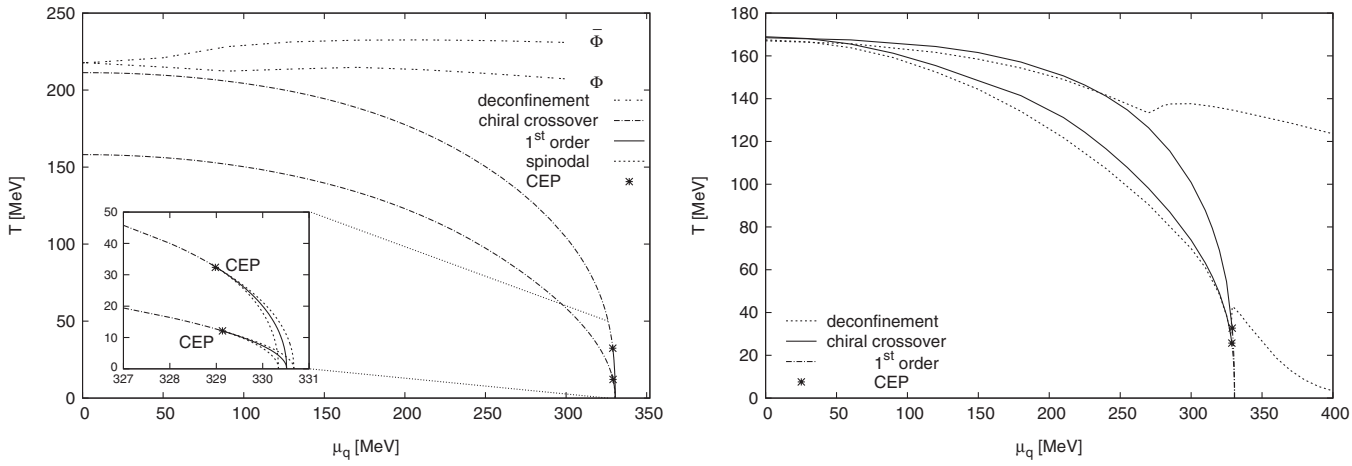

FIG. 4. Left panel: Phase diagrams obtained for the physical value of the pion mass using the local approximation to G_π with a mass determined by (33) without and with the inclusion of the Polyakov loop. The latter has higher $T_{\rm CEP}$ and was obtained using $U_{\rm poly}(\Phi, \bar{\Phi})$ with $T_0 = 270$ MeV. The part of the phase diagram where the transition is of first order is enlarged in the inset. Shown are the global maxima of $d\Phi(T)/dT$ and $d\bar{\Phi}(T)/dT$. Right panel: Chiral and deconfinement phase transitions obtained for $U_{\log}(\Phi, \bar{\Phi})$ with $T_0 = 208$ MeV (upper curves) and with $T_0(\mu_q)$ (lower curves). The deconfinement transition line is obtained from the global maximum of $d\Phi(T)/dT$.

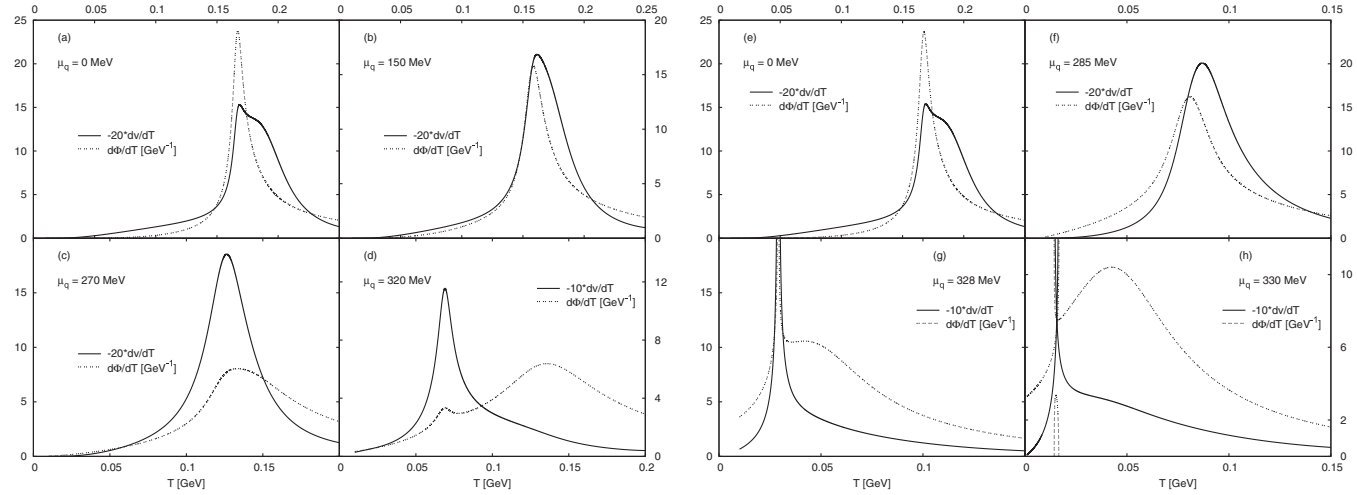

FIG. 5. Evolution of the maxima of the $-dv/dT$ and $d\Phi/dT$ with the increase of the chemical potential μ_q in case of using $U_{\log}(\Phi, \bar{\Phi})$ with a $T_0 = 208$ MeV (a)–(d) and with a μ_q-dependent T_0 parameter (e)–(h).

of the chiral transition on the shape of $d\Phi/dT$. This is the most pronounced in the case of the μ_q-dependent T_0 where the two transition lines cross near the CEP. In this case the chiral phase transition plays the driving role as one can clearly see in Fig. 5(g). In Fig. 5(d) one sees that $d\Phi/dT$ has two peaks. In such cases, as in Ref. [28], the position of the higher peak is followed to determine the deconfinement transition temperature, since the first peak is a result of the influence of the chiral phase transition.

From Table II one can see that there is a correlation between the strength of the chiral crossover at $\mu_q = 0$ as measured by Γ_χ and the location of CEP: weaker crossover (larger value of Γ_χ) corresponds in general to a larger value of μ_q^{CEP}. In the cases marked with an asterisk in Table II a dv/dT is distorted by the temperature dependence of the Polyakov loop, as one can see in Figs. 5(a) and 5(e). For this reason in this case we denote by Γ_χ the full width at half maximum of $-dv/dT$. In other cases one gives the half width at half maximum. This is measured on the left of the maximum, because when the gap equation is used, the threshold of the fermionic bubble is generally on the right of the maximum and distorts the dv/dT curve.

V. DISCUSSION AND CONCLUSIONS

Using the tree-level fermion propagator and several approximate forms of the pion propagator obtained within a large-N_f expansion, we studied in the chiral limit and for the physical value of the pion mass the influence of the Polyakov loop on the chiral phase transition. We obtained that only when the local part of the approximate pion propagator resums infinitely many orders in $1/N_f$ of fermionic contributions it is possible to find a CEP on the chiral phase transition line of the $\mu_q - T$ phase diagram. When the logarithmic form $U_{\log}(\Phi, \bar{\Phi})$ of the effective potential for the Polyakov loop was used with parameter $T_0 = 208$ MeV a crossing between the chiral and deconfinement transition lines was observed, with the latter line starting at $\mu_q = 0$ slightly below the former one. In this case the existence of the quarkyonic phase is possible.

We have seen at the beginning of Sec. IV B that as a result of resumming in the pion propagator $\mathcal{O}(1/\sqrt{N})$ fermionic fluctuations obtained with a strict expansion in $1/\sqrt{N}$, while keeping the fermion propagator unresummed, the phase transition softens. One can easily demonstrate the same feature by including the contributions of the fermion vacuum fluctuations and of the pion tadpole in the equation of state of Ref. [27], that is the field equation determining the chiral order parameter. There, because the parameters of the PQM model were determined at tree level, the fermionic vacuum fluctuations coming from the fermion tadpole ($\tilde{T}^0$) were neglected, while the pions were treated at tree level. However, by choosing an appropriate renormalization scale one can arrange for the vanishing of the entire $\tilde{T}_F^0$ only at $T = 0$. At finite temperature the vacuum fluctuation is in this way correctly included and due to the temperature dependent fermionic mass $\tilde{T}_F^0$ will be nonvanishing. The value of the renormalization scales for which the fermion and pion tadpoles vanish at $T = \mu_q = 0$ are $M_{0F} = \sqrt{e} m_q$ and $M_{0B} = \sqrt{e} m_\pi$, respectively. The importance of including the vacuum fluctuations was discussed also in [29,31], where the effect on the location of the CEP and on the isentropic trajectories in the $\mu_q - T$ plane was shown. From Table III one can see that comparing with the original result of Ref. [27] the inclusion of the fermionic vacuum fluctuations softens the transition at $\mu_q = 0$, as shown by the larger full width Γ_χ at half maximum of $-dv/dT$, and in consequence the location of the CEP is moved to higher values of μ_q and lower values of T. Inclusion of the pion vacuum and thermal fluctuations in the equation of state through a pion tadpole further accentuates this behavior.

TABLE III. The pseudocritical temperatures of the chiral transition and the full width Γ_χ at half maximum of $-dv/(dT)$ at $\mu_q = 0$, and the location of the CEP in units of MeV in various treatments of the model with a physical pion mass. The Polyakov loop is included using $U_{\rm poly}(\Phi, \bar{\Phi})$ and $T_0 = 208$ MeV. QP stands for the quasiparticle approximation in which the vacuum fluctuations in the fermion ($\tilde{T}_F^0$) or pion (T_F^0) tadpoles are disregarded (marked by $-$) and only the finite temperature part of the tadpoles ($\tilde{T}^\beta$ or T^β) is kept (marked by $+$). QFT stands for a quantum field theoretical calculation where the vacuum fluctuations are properly treated. The first row is the reproduced result of [27].

	$\tilde{T}_F^0$	T_F^0	$\tilde{T}^\beta$	T^β	$T_\chi(\mu_q = 0)$	Γ_χ	$T_{\rm CEP}$	$\mu_q^{\rm CEP}$
QP	$-$	$-$	$+$	$-$	184.6	4.6	162.8	165.1
QP	$-$	$-$	$+$	$+$	180.2	8.6	145.3	204.3
QFT	$+$	$-$	$+$	$-$	173.0	26.9	91.3	241.1
QFT	$+$	$+$	$+$	$+$	170.1	30.3	85.5	243.5

Inclusion of the fluctuations using functional renormalization group methods also pushed the location of the CEP to higher values of μ_q, as can be seen by comparing the left panel of Fig. 6 in [32] to Fig. 6 of [27].

It remains to be seen to what extent our results are stable against the use of the self-consistent propagator for fermions, as required by a completely systematic large-N_f expansion. A highly interesting question which requires going beyond the level of approximations of this work is whether a completely systematic expansion in $1/\sqrt{N}$ of the propagator equations could lead to the existence of the CEP in the phase diagram, and how the results obtained within such a resummation scheme are related to a numerically even more demanding resummation represented by the complete self-consistent solution (without further expansion in $1/\sqrt{N}$) of the coupled pion and fermion propagator equations.

ACKNOWLEDGMENTS

The authors benefited from discussions with András Patkós and Antal Jakovác. This work is supported by the Hungarian Research Fund under Contracts No. T068108 and No. K77534.

APPENDIX: INTEGRALS AND PERFORMING THE COLOR TRACE

1. The trace log

We calculate first an integral appearing in (18) when the approximation $G(k) \to D(k)$ is used. This is defined as

$$I_1 = \sqrt{N} i \,\mathrm{tr}_{D,c} \int_k \ln D^{-1}(k) = -2\sqrt{N} T \sum_{i=1}^{N_c} \sum_n \int \frac{d^3\mathbf{k}}{(2\pi)^3} \ln[\beta^2(\omega_n^2 + E_k^2)], \quad \text{(A1)}$$

where we used (21) and the notation $E_k^2 = \mathbf{k}^2 + m_q^2$. The Matsubara frequencies are $\omega_n = (2n+1)\pi T - i\mu_i$, with the color-dependent chemical potentials defined in (15). Doing the Matsubara sum and an integration by parts one obtains

$$I_1 = -2\sqrt{N} \sum_{i=1}^{N_c} \int \frac{d^3\mathbf{k}}{(2\pi)^3} \left[E_k + \frac{k^2}{3E_k} (\tilde{f}_i^+(E_k) + \tilde{f}_i^-(E_k)) \right], \quad \text{(A2)}$$

where $\tilde{f}_i^\pm(E) = 1/(\exp[\beta(E \mp \mu_i)] + 1)$. Using the diagonal form of the Polyakov-loop operator given in (2) one can define following Ref. [16]

$$\tilde{f}_\Phi^+(E) = \frac{1}{N_c} \sum_{i=1}^{N_c} \tilde{f}_i^+(E) = \frac{1}{N_c} \,\mathrm{tr}_c \frac{1}{L e^{\beta(E-\mu_q)} + 1}, \quad \text{(A3a)}$$

$$\tilde{f}_\Phi^-(E) = \frac{1}{N_c} \sum_{i=1}^{N_c} \tilde{f}_i^-(E) = \frac{1}{N_c} \,\mathrm{tr}_c \frac{1}{L^\dagger e^{\beta(E+\mu_q)} + 1}. \quad \text{(A3b)}$$

Then, simple algebra shows that upon working out the traces $\tilde{f}_\Phi^\pm(E)$ can be expressed in terms of $\Phi = (\mathrm{tr}_c L)/N_c$ and $\bar{\Phi} = (\mathrm{tr}_c L^\dagger)/N_c$ as

$$\tilde{f}_\Phi^+(E) = \frac{(\bar{\Phi} + 2\Phi e^{-\beta(E-\mu_q)}) e^{-\beta(E-\mu_q)} + e^{-3\beta(E-\mu_q)}}{1 + 3(\bar{\Phi} + \Phi e^{-\beta(E-\mu_q)}) e^{-\beta(E-\mu_q)} + e^{-3\beta(E-\mu_q)}}, \quad \text{(A4a)}$$

$$\tilde{f}_\Phi^-(E) = \frac{(\Phi + 2\bar{\Phi} e^{-\beta(E+\mu_q)}) e^{-\beta(E+\mu_q)} + e^{-3\beta(E+\mu_q)}}{1 + 3(\Phi + \bar{\Phi} e^{-\beta(E+\mu_q)}) e^{-\beta(E+\mu_q)} + e^{-3\beta(E+\mu_q)}}. \quad \text{(A4b)}$$

Through these functions the integral I_1 in (A1) is also expressed in terms of Φ and $\bar{\Phi}$ as

$$I_1 = -2N_c\sqrt{N}\int\frac{d^3\mathbf{k}}{(2\pi)^3}\left[E_k + \frac{k^2}{3E_k}(\tilde{f}^+_\Phi(E_k) + \tilde{f}^-_{\bar\Phi}(E_k))\right]. \tag{A5}$$

The derivative of this integral with respect to Φ is used in (55).

2. Tadpole and bubble integrals

The pion tadpole integral is given by

$$\begin{aligned} T(M) &= \int_k G_{\pi,l}(k) = T\sum_n\int_{\mathbf{k}}\frac{1}{E_k^2+\omega_n^2} \\ &= T_{\rm div}(M) + T_F(M), \end{aligned} \tag{A6}$$

where $\omega_n = 2\pi nT$ and $E_k^2 = \mathbf{k}^2 + M^2$. Depending on which one of the approximated pion propagators discussed in Sec. II D is used, the T-dependent mass M satisfies either one of the gap equations (32) and (33), or (43a), or the relation $M^2 = h/\upsilon$. Using a 4D cutoff Λ in Euclidean space, the quadratic and logarithmic divergences,

$$\begin{aligned} T_d^{(2)} &= \frac{1}{16\pi^2}\left[\Lambda^2 - M_0^2\ln\frac{\Lambda^2}{M_0^2}\right], \\ T_d^{(0)} &= -\frac{1}{16\pi^2}\ln\frac{\Lambda^2}{M_0^2}, \end{aligned} \tag{A7}$$

are separated in the divergent part

$$T_{\rm div}(M) = T_d^{(2)} + [M^2 - M_0^2]T_d^{(0)}, \tag{A8}$$

by expanding, as in Appendix A of [71], the propagator $G_{\pi,l}(k)$ around the auxiliary propagator

$$G_0(p) = \frac{i}{p^2 - M_0^2}. \tag{A9}$$

Here, $M_0^2 = M_{0B}^2/e$, where M_{0B} is the renormalization scale introduced in Sec. II E.

The finite part of the tadpole is written as a sum of two terms, having zero and one statistical factors, respectively

$$\begin{aligned} T_F(M) &= T_F^0(M) + T^\beta(M), \qquad T_F^0(M) = \frac{M^2}{16\pi^2}\ln\frac{eM^2}{M_{0B}^2}, \\ T^\beta(M) &= \int\frac{d^3\mathbf{k}}{(2\pi)^3}\frac{f(E_k)}{E_k}, \end{aligned} \tag{A10}$$

where $f(E) = 1/(\exp(\beta E) - 1)$.

The fermion tadpole integral defined in Eq. (26) is written as

$$\tilde{T}(m_q) = \frac{T}{N_c}\sum_{i=1}^{N_c}\sum_n\int_{\mathbf{k}}\frac{1}{E_k^2+\omega_n^2} = \tilde{T}_{\rm div}(m_q) + \tilde{T}_F(m_q), \tag{A11}$$

where $E_k^2 = \mathbf{k}^2 + m_q^2$, $\omega_n = (2n+1)\pi T - i\mu_i$. The sum over the color degrees of freedom was done with the help of (A3). The divergent part of $\tilde{T}(m_q)$ reads

$$\tilde{T}_{\rm div}(m_q) = T_d^{(2)} + [m_q^2 - M_0^2]T_d^{(0)}, \tag{A12}$$

while the finite part is decomposed as in (A10):

$$\begin{aligned} \tilde{T}_F(m_q) &= \tilde{T}_F^0(m_q) + \tilde{T}^\beta(m_q), \\ \tilde{T}_F^0(m_q) &= \frac{m_q^2}{16\pi^2}\ln\frac{em_q^2}{M_{0B}^2}, \\ \tilde{T}^\beta(m_q) &= -\int\frac{d^3\mathbf{k}}{(2\pi)^3}\frac{1}{2E_k}(\tilde{f}^+_\Phi(E_k) + \tilde{f}^-_\Phi(E_k)), \end{aligned} \tag{A13}$$

with $\tilde{f}^\pm_\Phi(E_k)$ given in (A4).

The fermion bubble integral given in Eq. (27) is decomposed as

$$\begin{aligned} \tilde{I}(p;m_q) &= -\frac{T}{N_c}\sum_{i=1}^{N_c}\sum_n\int_{\mathbf{k}}\frac{1}{[E_1^2+\omega_n^2][E_2^2+(\omega_n - ip_0)^2]} \\ &= \tilde{I}_{\rm div}(p;m_q) + \tilde{I}_F(p;m_q), \end{aligned} \tag{A14}$$

where $E_1^2 = \mathbf{k}^2 + m_q^2$, $E_2^2 = (\mathbf{k}-\mathbf{p})^2 + m_q^2$, and $\omega_n = (2n+1)\pi T - i\mu_i$. The divergent part obtained after doing the Matsubara sum is independent of the momentum and is given by

$$\tilde{I}_{\rm div}(p;m_q) = T_d^{(0)}, \tag{A15}$$

while the finite part is written again as a sum of two terms, having zero and one statistical factor, respectively:

$$\tilde{I}_F(p;m_q) = \tilde{I}_F^0(p;m_q) + \tilde{I}^\beta(p;m_q). \tag{A16}$$

The finite part with no statistical factor is given by

$$\begin{aligned} \tilde{I}_F^0(p;m_q) &= \frac{1}{16\pi^2}\ln\frac{m_q^2}{M_0^2} \\ &\quad + \frac{Q}{16\pi^2}\begin{cases} 2\arctan Q^{-1}, & 0 < p^2 < 4m_q^2, \\ -\ln\frac{Q-1}{Q+1}, & p^2 < 0,\ p^2 > 4m_q^2, \end{cases} \end{aligned} \tag{A17}$$

where $Q = \sqrt{|1 - 4m_q^2/p^2|}$, while, after summing over color indices, the term with the statistical factor reads

$$\tilde{I}^{\beta}(p;m_q) = -\int_{\mathbf{k}} \frac{1}{4E_1E_2}\Big[\frac{\tilde{f}^{+}_{\Phi}(E_1)+\tilde{f}^{-}_{\Phi}(E_2)}{p_0-E_1-E_2+i\epsilon} - \frac{\tilde{f}^{-}_{\Phi}(E_1)+\tilde{f}^{+}_{\Phi}(E_2)}{p_0+E_1+E_2+i\epsilon} - \frac{\tilde{f}^{+}_{\Phi}(E_1)-\tilde{f}^{+}_{\Phi}(E_2)}{p_0-E_1+E_2+i\epsilon} + \frac{\tilde{f}^{-}_{\Phi}(E_1)-\tilde{f}^{-}_{\Phi}(E_2)}{p_0+E_1-E_2+i\epsilon}\Big]. \quad \text{(A18)}$$

3. The setting-sun integral

Using the definitions of the fermion bubble integral given in (27) together with the relations (A14) and (A15), the integral defined in (36) reads in terms of the propagator D_0 introduced in (25) as

$$J(M,m_q) = -\frac{1}{N_c}\sum_{i=1}^{N_c}\int_p G^2_{\pi,l}(p)p^2\int_q D_0(q)D_0(q+p) + iT^{(0)}_d\int_p p^2G^2_{\pi,l}(p) = \Big[1+M^2\frac{d}{dM^2}\Big](S(M,m_q)-T(M)T^{(0)}_d). \quad \text{(A19)}$$

Here, we have used that $-i\int_p G^2_{\pi,l}(p) = dT(M)/(dM^2)$, with M satisfying the relation $M^2 = h/\upsilon$ or the gap equation (43a) and we introduced the setting-sun integral

$$S(M,m_q) = \frac{1}{N_c}\sum_{i=1}^{N_c}\Big[-i\int_k\int_q D_0(k)G_{\pi,l}(q)D_0(k+q)\Big]. \quad \text{(A20)}$$

With the method described in Refs. [70,77] the setting-sun integral can be decomposed as a sum of terms containing zero, one, and two statistical factors:

$$S(M,m_q) = S^0(M,m_q) + S^{\beta,1}(M,m_q) + S^{\beta,2}(M,m_q), \quad \text{(A21)}$$

with

$$S^0(M,m_q) = -i\int^{(0)}_k\int^{(0)}_q D_0(k)G_{\pi,l}(q)D_0(k+q), \quad \text{(A22a)}$$

$$S^{\beta,1}(M,m_q) = \frac{1}{N_c}\sum_{i=1}^{N_c}\int^{(0)}_k[\tilde{I}^0(k;m_q)\sigma(k) - 2I^0_{q\pi}(k)\tilde{\sigma}_i(k)] = [T^{\beta}(M)+2\tilde{T}^{\beta}(m_q)]T^{(0)}_d + S^{\beta,1}_F(M,m_q), \quad \text{(A22b)}$$

$$S^{\beta,2}(M,m_q) = -\frac{i}{N_c}\sum_{i=1}^{N_c}\int^{(0)}_k\int^{(0)}_q[\tilde{\sigma}_i(k)\tilde{\sigma}_i(q)G_{\pi,l}(k+q) - 2\tilde{\sigma}_i(k)\sigma(q)D_0(k+q)], \quad \text{(A22c)}$$

where $\tilde{\sigma}_i(k) = \epsilon(k_0)\tilde{\rho}_0(k)(\tilde{f}^{+}_i(|k_0|)+\tilde{f}^{-}_i(|k_0|))/2$ and $\sigma(k) = \epsilon(k_0)\tilde{\rho}_0(k)f(|k_0|)$, with $\epsilon(k_0)$ the sign function, and $\tilde{\rho}_0(k) = 2\pi\epsilon(k_0)\delta(k^2-m_q^2)$ and $\rho_0(k) = 2\pi\epsilon(k_0)\delta(k^2-M^2)$ the free spectral functions. Here, we have introduced the notation $\int^{(0)}_k = \int\frac{d^4k}{(2\pi)^4}$ and we have separated in $S^{\beta,1}$ the divergence coming from (A14) and

$$I^0_{q\pi}(k) = -i\int^{(0)}_q G_{\pi,l}(q)D_0(k+q) = T^{(0)}_d + I^0_{q\pi,F}(k), \quad \text{(A23)}$$

where the finite part is

$$I^0_{q\pi,F}(k) = \frac{1}{32\pi^2}\Big[\Big(1+\frac{\Delta m^2}{k^2}\Big)\ln\frac{M^2}{M_0^2} + \Big(1-\frac{\Delta m^2}{k^2}\Big)\ln\frac{m_q^2}{M_0^2}\Big] + \frac{G}{16\pi^2k^2}\begin{cases} -\frac{1}{2}\ln\frac{M^2+m_q^2-k^2+G}{M^2+m_q^2-k^2-G} - i\pi\Theta(k^2-(M+m_q)^2), & k^2>(M+m_q)^2, k^2<(M-m_q)^2, \\ \arctan\frac{k^2+\Delta m^2}{G} + \arctan\frac{k^2-\Delta m^2}{G}, & (M-m_q)^2<k^2<(M+m_q)^2, \end{cases} \quad \text{(A24)}$$

with $\Delta m^2 = M^2 - m_q^2$ and $G = \sqrt{p^4 - 2p^2(M^2+m_q^2)+(M^2-m_q^2)^2}$.

In $S^0(M,m_q)$ one expands, as in Ref. [71], the propagators $G_{\pi,l}$ and D_0 around the auxiliary propagator defined in (A9) and one obtains

$$S^0(M,m_q) = S^0(M_0) + [T^0(M)+2\tilde{T}^0(m_q)-3T^{(2)}_d]T^{(0)}_d + [M^2-M_0^2+2(m_q^2-M_0^2)]T^{(I)}_d + S^0_F(M,m_q), \quad \text{(A25)}$$

where

$$T^{(I)}_d = -i\int^{(0)}_p G^2_0(p)\Big[-i\int^{(0)}_q G_0(q)G_0(q+p) - T^0_d\Big] = \frac{1}{3}\frac{dS^0(M_0)}{dM_0^2} - [T^{(0)}_d]^2 - \frac{T^{(0)}_d}{16\pi^2}. \quad \text{(A26)}$$

The divergent parts of S^0 and $S^{\beta,1}$ combine, so that the complete divergence of the setting-sun integral reads

$$S_{\rm div}(M,m_q) = S^0_{\rm div}(M,m_q) + S^{\beta,1}_{\rm div}(M,m_q) = S^0(M_0) + [T(M) + 2\tilde{T}(m_q) - 3T_d^{(2)}]T_d^{(0)} + [M^2 + 2m_q^2 - 3M_0^2)]T_d^{(I)}. \quad \text{(A27)}$$

Using this expression in (A19) one obtains

$$J_{\rm div}(M,m_q) = S^0(M_0) + [2\tilde{T}(m_q) - 3T_d^{(2)}]T_d^{(0)} + [2(M^2 + m_q^2) - 3M_0^2]T_d^{(I)}. \quad \text{(A28)}$$

In what follows we give the finite part of the setting-sun integral in terms of which $J_F(M,m_q)$ can be easily obtained. With the help of (A26) one obtains from (A25)

$$S_F^0(M,m_q) = S^0(M,m_q) - S^0(M_0) - \frac{1}{3}[M^2 + 2m_q^2 - 3M_0^2] \times \frac{dS^0(M_0)}{dM_0^2} - \frac{T_d^{(0)}}{16\pi^2}\Big[M^2 \ln\frac{M^2}{eM_0^2} + 2m_q^2 \ln\frac{m_q^2}{eM_0^2} + 3M_0^2\Big]. \quad \text{(A29)}$$

$S_F^0(M,m_q)$ can be most easily calculated numerically as in [78] by going to Euclidean space and using 4D cutoff Λ to regularize the integrals. By doing the angular integration one obtains

$$S^0(M,m_q) = -\frac{1}{2^9\pi^4}\int_0^{\Lambda^2} dx \int_0^{\Lambda^2} dy \times \frac{x + y + m_q^2 - \sqrt{(x + y + m_q^2)^2 - 4xy}}{(x + m_q^2)(y + M^2)}, \quad \text{(A30)}$$

with a similar integral for $S^0(M)$, but with m_q replaced by M_0. Then, by calculating $T_d^{(0)}$ defined in (A7) with the same cutoff Λ, one can look for the range of Λ where $S_F^0(M,m_q)$ is insensitive to the variation of Λ. In this work we have used $\Lambda \in [600, 800]$ GeV.

The finite part of the setting-sun integral with one statistical factor factorizes upon integration over k_0 due to the Dirac delta's of the free spectral functions and one has

$$S_F^{\beta,1}(M,m_q) = \tilde{I}_F^0(k^2 = M^2, m_q)T^\beta(M) + 2I^0_{q\pi,F}(k^2 = m_q^2)\tilde{T}^\beta(m_q). \quad \text{(A31)}$$

After performing the frequency and angular integrals in the part of the setting-sun integral containing two statistical factors one obtains

$$S^{\beta,2}(M,m_q) = -\frac{1}{64\pi^4}\frac{1}{N_c}\sum_{i=1}^{N_c}\int_0^\infty d|\mathbf{k}| \int_0^\infty |\mathbf{q}||\mathbf{k}||\mathbf{q}|\Big\{-\frac{2}{E_1E}(\tilde{f}_i^+(E_1) + \tilde{f}_i^-(E_1))f(E) \times \Big[\ln\Big|\frac{(E_1+E)^2 - E_+^2}{(E_1+E)^2 - E_-^2}\Big| + \ln\Big|\frac{(E_1-E)^2 - E_+^2}{(E_1-E)^2 - E_-^2}\Big|\Big] + \frac{1}{E_1E_2}\Big[(\tilde{f}_i^+(E_1)\tilde{f}_i^-(E_2) + \tilde{f}_i^-(E_1)\tilde{f}_i^+(E_2)) \times \ln\Big|\frac{(E_1+E_2)^2 - \bar{E}_+^2}{(E_1+E_2)^2 - \bar{E}_-^2}\Big| + (\tilde{f}_i^+(E_1)\tilde{f}_i^+(E_2) + \tilde{f}_i^-(E_1)\tilde{f}_i^-(E_2))\ln\Big|\frac{(E_1-E_2)^2 - \bar{E}_+^2}{(E_1-E_2)^2 - \bar{E}_-^2}\Big|\Big]\Big\}, \quad \text{(A32)}$$

where $E_1 = \sqrt{\mathbf{k}^2 + m_q^2}$, $E_2 = \sqrt{\mathbf{q}^2 + m_q^2}$, $E = \sqrt{\mathbf{q}^2 + M^2}$, and $E_\pm = \sqrt{(|\mathbf{k}| \pm |\mathbf{q}|)^2 + M^2}$, $\bar{E}_\pm = \sqrt{(|\mathbf{k}| \pm |\mathbf{q}|)^2 + m_q^2}$. For the terms containing one fermionic statistical factor the sum over color indices will give the functions $\tilde{f}^\pm_\Phi$ introduced in (A4). For the terms containing two fermionic statistical factors one introduces the notation $X_\pm = \exp[\beta(E_1 \mp \mu_q)]$ and $Y_\pm = \exp[\beta(E_2 \mp \mu_q)]$ and writes the statistical factors in terms of the Polyakov-loop operator. One obtains

$$\frac{1}{N_c}\sum_{i=1}^{N_c}\tilde{f}_i^+(E_1)\tilde{f}_i^-(E_2) = \frac{1}{N_c}\sum_{i=1}^{N_c}\mathrm{tr}_c\Big[\frac{1}{LX_+ + 1}\frac{1}{L^\dagger Y_- + 1}\Big] = \frac{1 + X_+Y_-(1 + X_+Y_-) + \bar{\Phi}[2Y_-(1 + X_+Y_-) + X_+^2] + \Phi[2X_+(1 + X_+) + Y_-^2] + 3\Phi\bar{\Phi}X_+Y_-}{(X_+^3 + 3\bar{\Phi}X_+^2 + 3\Phi X_+ + 1)(Y_-^3 + 3\Phi Y_-^2 + 3\bar{\Phi}Y_- + 1)}. \quad \text{(A33)}$$

For the term with $\tilde{f}_i^-(E_1)\tilde{f}_i^+(E_2)$ one obtains the same expression, but with X_+ replaced by Y_+ and Y_- replaced by X_-. Similarly, one has

$$\frac{1}{N_c}\sum_{i=1}^{N_c}\tilde{f}_i^+(E_1)\tilde{f}_i^+(E_2) = \frac{3\bar{\Phi}^2X_+^2Y_+^2 + 6\Phi^2X_+Y_+ + (3\Phi\bar{\Phi} - 1)X_+Y_+(X_+ + Y_+) + 2\Phi(X_+ + Y_+ - X_+^2Y_+^2) + \bar{\Phi}(X_+ - Y_+)^2 + 1}{(X_+^3 + 3\bar{\Phi}X_+^2 + 3\Phi X_+ + 1)(Y_+^3 + 3\bar{\Phi}Y_+^2 + 3\Phi Y_+ + 1)}, \quad \text{(A34)}$$

and for the term with $\tilde{f}_i^-(E_1)\tilde{f}_i^-(E_2)$ one has the same expression, but with $\bar{\Phi}$ interchanged with Φ, and X_+ replaced by X_- and Y_+ replaced by Y_-. We note here that, as one can see by setting $\Phi = \bar{\Phi} = 0$, the expression on the right-hand side of (A34) can be negative and in consequence it does not allow for an interpretation in terms of distribution functions.

When the approximation $G(k) \to D(k)$ is used, the setting-sun integral defined in (A20) appears also in the expression of the quark-pion two-loop integral of (18) which reads

$$I_2 = -\sqrt{N}\frac{g^2}{2} i \,\mathrm{tr}_{D,c} \int_k \int_p \gamma_5 D(k)\gamma_5 D(k+p) G_{\pi,l}(p) = g^2\sqrt{N}N_c[\tilde{T}_2(m_q) - 2\tilde{T}(m_q)T(M) - M^2 S(M, m_q)], \tag{A35}$$

where depending on the approximation on the pion propagator M satisfies either one of the gap equations (32), (33), and (43a) or the relation $M^2 = h/\upsilon$. Here, we introduced the integral

$$\tilde{T}_2(m_q) = \frac{1}{N_c}\sum_{i=1}^{N_c}\Big[-i\int_k\int_q D_0(k)D_0(q)\Big], \tag{A36}$$

which, after performing the Matsubara sums, can be written as

$$\tilde{T}_2(m_q) = \tilde{T}_2^0(m_q) + \tilde{T}_2^{\beta,1}(m_q) + \tilde{T}_2^{\beta,2}(m_q), \tag{A37a}$$

$$\tilde{T}_2^0(m_q) = (\tilde{T}(m_q))^2, \qquad \tilde{T}_2^{\beta,1}(m_q) = 2\tilde{T}^0(m_q)\tilde{T}^\beta(m_q) \tag{A37b}$$

$$\tilde{T}_2^{\beta,2}(m_q) = \frac{1}{16\pi^4}\int_0^\infty d|\mathbf{k}|\int_0^\infty d|\mathbf{q}| \times \frac{k^2q^2}{E_1E_2}\sum_{r,s=\pm}\Big[\frac{1}{N_c}\sum_{i=1}^{N_c}\tilde{f}_i^r(E_1)\tilde{f}_i^s(E_2)\Big], \tag{A37c}$$

where $E_1 = \sqrt{\mathbf{k}^2 + m_q^2}$, $E_2 = \sqrt{\mathbf{q}^2 + m_q^2}$, and the color sums are given in (A33) and (A34). In terms of the quantities defined in (A37) the derivative with respect to Φ of I_2 appears in (55).

[1] Y. Nambu and G. Jona-Lasinio, Phys. Rev. **122**, 345 (1961).
[2] M. Gell-Mann and M. Levy, Nuovo Cimento **16**, 705 (1960).
[3] E. Megías, E. R. Arriola, and L. L. Salcedo, Phys. Rev. D **74**, 065005 (2006).
[4] A. Casher, Phys. Lett. **83B**, 395 (1979).
[5] T. Banks and A. Casher, Nucl. Phys. **B169**, 103 (1980).
[6] R. G. Edwards, U. M. Heller, J. Kiskis, and R. Narayanan, Phys. Rev. D **61**, 074504 (2000).
[7] T. G. Kovács, Proc. Sci., LATTICE2008 (2008) 198.
[8] C. Gattringer, Phys. Rev. Lett. **97**, 032003 (2006).
[9] S. Chandrasekharan and N. Christ, Nucl. Phys. B, Proc. Suppl. **47**, 527 (1996).
[10] M. A. Stephanov, Phys. Lett. B **375**, 249 (1996).
[11] L. Ya. Glozman, Phys. Rev. D **80**, 037701 (2009).
[12] L. McLerran and R. D. Pisarski, Nucl. Phys. **A796**, 83 (2007).
[13] K. Fukushima, Phys. Lett. B **591**, 277 (2004).
[14] P. N. Meisinger and M. C. Ogilvie, Phys. Lett. B **379**, 163 (1996).
[15] S. Chandrasekharan and S. Huang, Phys. Rev. D **53**, 5100 (1996).
[16] H. Hansen, W. M. Alberico, A. Beraudo, A. Molinari, M. Nardi, and C. Ratti, Phys. Rev. D **75**, 065004 (2007).
[17] H. Abuki, R. Anglani, R. Gatto, G. Nardulli, and M. Ruggieri, Phys. Rev. D **78**, 034034 (2008).
[18] K. Kashiwa, H. Kouno, M. Matsuzaki, and M. Yahiro, Phys. Lett. B **662**, 26 (2008).
[19] P. Costa, C. A. de Sousa, M. C. Ruivo, and H. Hansen, Europhys. Lett. **86**, 31001 (2009).
[20] Y. Sakai, K. Kashiwa, H. Kouno, M. Matsuzaki, and M. Yahiro, Phys. Rev. D **79**, 096001 (2009).
[21] M. Ciminale, R. Gatto, N. D. Ippolito, G. Nardulli, and M. Ruggieri, Phys. Rev. D **77**, 054023 (2008).
[22] W. J. Fu, Z. Zhang, and Y. X. Liu, Phys. Rev. D **77**, 014006 (2008).
[23] P. Costa, M. C. Ruivo, C. A. de Sousa, H. Hansen, and W. M. Alberico, Phys. Rev. D **79**, 116003 (2009).
[24] C. Sasaki, B. Friman, and K. Redlich, Phys. Rev. D **75**, 074013 (2007).
[25] G. A. Contrera, D. Gómez Dumm, and N. N. Scoccola, Phys. Rev. D **81**, 054005 (2010).
[26] L. McLerran, K. Redlich, and C. Sasaki, Nucl. Phys. **A824**, 86 (2009).
[27] B.-J. Schaefer, J. M. Pawlowski, and J. Wambach, Phys. Rev. D **76**, 074023 (2007).
[28] T. Kähärä and K. Tuominen, Phys. Rev. D **78**, 034015 (2008).
[29] E. Nakano, B.-J. Schaefer, B. Stokic, B. Friman, and K. Redlich, Phys. Lett. B **682**, 401 (2010).
[30] V. Skokov, B. Stokic, B. Friman, and K. Redlich, Phys. Rev. C **82**, 015206 (2010).
[31] V. Skokov, B. Friman, E. Nakano, K. Redlich, and B.-J. Schaefer, Phys. Rev. D **82**, 034029 (2010).
[32] T. Herbst, J. Pawlowski, and B.-J. Schaefer, arXiv:1008.0081.
[33] B.-J. Schaefer, M. Wagner, and J. Wambach, Phys. Rev. D **81**, 074013 (2010).
[34] H. Mao, J. Jin, and M. Huang, J. Phys. G **37**, 035001 (2010).
[35] U. S. Gupta and V. K. Tiwari, Phys. Rev. D **81**, 054019 (2010).
[36] A. J. Mizher, M. N. Chernodub, and E. S. Fraga, arXiv:1004.2712.

[37] A. Mócsy, F. Sannino, and K. Tuominen, J. High Energy Phys. 03 (2004) 044.
[38] E. Fraga and A. Mócsy, Braz. J. Phys. **37**, 281 (2007).
[39] W. Weise, Prog. Theor. Phys. Suppl. **174**, 1 (2008).
[40] A. Jakovác, A. Patkós, Zs. Szép, and P. Szépfalusy, Phys. Lett. B **582**, 179 (2004).
[41] H. Reinhardt, Nucl. Phys. **B503**, 505 (1997).
[42] C. Ford, U. G. Mitreuter, J. Pawlowski, T. Tok, and A. Wipf, Ann. Phys. (N.Y.) **269**, 26 (1998).
[43] M. Schaden, Phys. Rev. D **71**, 105012 (2005).
[44] G. 't Hooft, Nucl. Phys. **B138**, 1 (1978).
[45] L. D. McLerran and B. Svetitsky, Phys. Rev. D **24**, 450 (1981).
[46] B. Svetitsky, Phys. Rep. **132**, 1 (1986).
[47] M. Faber, O. Borisenko, S. Mashkevich, and G. Zinovjev, Nucl. Phys. B, Proc. Suppl. **42**, 484 (1995).
[48] S. Kratochvila and Ph. de Forcrand, Phys. Rev. D **73**, 114512 (2006).
[49] O. Kaczmarek, F. Karsch, P. Petreczky, and F. Zantow, Phys. Lett. B **543**, 41 (2002).
[50] R. D. Pisarski, Phys. Rev. D **62**, 111501(R) (2000).
[51] C. Ratti, M. A. Thaler, and W. Weise, Phys. Rev. D **73**, 014019 (2006).
[52] G. Boyd, J. Engels, F. Karsch, E. Laermann, C. Legeland, M. Lütgemeier, and B. Petersson, Nucl. Phys. **B469**, 419 (1996).
[53] K. Fukushima, Prog. Theor. Phys. **153**, 204 (2004).
[54] C. Ratti, S. Rößner, M. A. Thaler, and W. Weise, Eur. Phys. J. C **49**, 213 (2007).
[55] S. Rößner, C. Ratti, and W. Weise, Phys. Rev. D **75**, 034007 (2007).
[56] K. Fukushima, Phys. Rev. D **77**, 114028 (2008).
[57] W. A. Bardeen and B. W. Lee, Phys. Rev. **177**, 2389 (1969).
[58] D. Röder, J. Ruppert, and D. H. Rischke, Phys. Rev. D **68**, 016003 (2003).
[59] A. Patkós, Zs. Szép, and P. Szépfalusy, Phys. Lett. B **537**, 77 (2002).
[60] G. Fejős and A. Patkós, Phys. Rev. D **82**, 045011 (2010).
[61] C. P. Korthals Altes, R. D. Pisarski, and A. Sinkovics, Phys. Rev. D **61**, 056007 (2000).
[62] J. M. Luttinger and J. C. Ward, Phys. Rev. **118**, 1417 (1960).
[63] D. Dominici and U. Marini Bettolo Marconi, Phys. Lett. B **319**, 171 (1993).
[64] G. Fejős, A. Patkós, and Zs. Szép, Phys. Rev. D **80**, 025015 (2009).
[65] J. Zinn-Justin, *Quantum Field Theory and Critical Phenomena* (Oxford University Press, Oxford, 2002), 4th ed.
[66] I. Caprini, G. Colangelo, and H. Leutwyler, Phys. Rev. Lett. **96**, 132001 (2006).
[67] H. van Hees and J. Knoll, Phys. Rev. D **65**, 105005 (2002).
[68] J.-P. Blaizot, E. Iancu, and U. Reinosa, Nucl. Phys. **A736**, 149 (2004).
[69] J. Berges, Sz. Borsányi, U. Reinosa, and J. Serreau, Ann. Phys. (N.Y.) **320**, 344 (2005).
[70] U. Reinosa, Nucl. Phys. **A772**, 138 (2006).
[71] A. Patkós and Zs. Szép, Nucl. Phys. **A811**, 329 (2008).
[72] A. Jakovác, Phys. Rev. D **78**, 085013 (2008).
[73] G. Fejős, A. Patkós, and Zs. Szép, Nucl. Phys. **A803**, 115 (2008).
[74] G. Weiglein, R. Scharf, and M. Böhm, Nucl. Phys. **B416**, 606 (1994).
[75] Z. Fodor, S. D. Katz, and C. Schmidt, J. High Energy Phys. 03 (2007) 121.
[76] K. Moura, T. Z. Nakano, and A. Ohnishi, Prog. Theor. Phys. **122**, 1045 (2009).
[77] J.-P. Blaizot and U. Reinosa, Nucl. Phys. **A764**, 393 (2006).
[78] J.-F. Yang, J. Zhou, and Chen Wu, Commun. Theor. Phys. **40**, 461 (2003) [http://ctp.itp.ac.cn/search.asp].